strongly indicates that forces exerted by the cytoskeleton are important in the detachment process.[72] Yamato *et al.* also found that the detachment of fibronectin from PIPAAm surfaces was unable to be induced by the hydration of PIPAAm chains.[71] Cellular activity can be categorized into two classes: one is chemical (the degradation of matrix components by matrix metalloproteinases and covalently crosslinking by transglutaminase) and the other physical (traction forces). Based on the knowledge described above and their results regarding cell detachment from PIPAAm surfaces, the active step (the first step) is thought to be mainly caused by chemical cellular activity, followed by the fully detachment by physical traction force due to the hydration of PIPAAm chain.[71]

The mechanism of cell detachment from PIPAAm-grafted surfaces was also investigated through the observations of collagen type IV.[68] Immunofluorescence study revealed that relatively little collagen was left beneath the center of each cell and more collagen was remained beneath the cells' edges. This difference was much consistence with a two-step mechanism of cell detachment. In the first step, cell actively detaches from its ECM on the cell edges only, followed by the complete detachment of the rest part of the cell from the surface, with its ECM attached to the cells.

ECM deposited beneath the cultured cells and cell sheet is a subject of investigation by many research groups. As one of the functions of ECM is anchoring and providing support for cells, a method allowing cells to detach from their culture surfaces with intact ECM is desirable.

The amounts of FN present in ECM of cultured cells before and after low-temperature detachment from PIPAAm-grafted surface was investigated by Kushida *et al.* in 1999.[32] Immunofluorescence study of ECs growing on PIPAAm-grafted surfaces showed that cells adhered, spread, and deposited FN on PIPAAm surfaces over the time of the culture. After reducing the temperature, intact cell sheets detached themselves from the grafted surfaces. Immunostaining assay of the detached sheets revealed that a majority of FN detached together with the cell sheets (Fig. 4). The area where the cells detached was found to show no FN. In comparison, after treatment with trypsin, FN was only faintly detected. Physical scraping recovered the comparable amounts of FN to low-temperature treatment.

The results of MDCK cell detachment from PIPAAm grafted surfaces performed by Kushida *et al.* are much consistent with those of ECs detachment.[33]

Canavan *et al.* investigated the location of laminin, fibronectin, and type I and type IV collagens after cell detachment from plasma polymerized PIPAAm.[5–7] Immunoassays revealed that most fibronectin and laminin detached together with the cell sheets after reducing temperature. According to ToF-SIMS, glycine and proline were left on the surfaces after cell recovery. Since these amino acids are the main composition of collagen, it was indicated that some collagen may remain on the surface after the detachment.[7] XPS analyses also showed that, when the cell sheets were lifted off PIPAAm-grafted TCPS, some residual proteins and/or peptides were left behind. A comparison of the molar ratio of amide species estimated from the C1s spectrum before and after cell culture also suggested that PIPAAm grafted by EB irradiation could reduce protein and/or peptide absorption more efficiently than that grafted by plasma method.[7] Although the difference between the two methods is unclear, we speculate that EB irradiation method provides a more uniform grafting of PIPAAm on TCPS surfaces than the method of plasma polymerization PIPAAm.

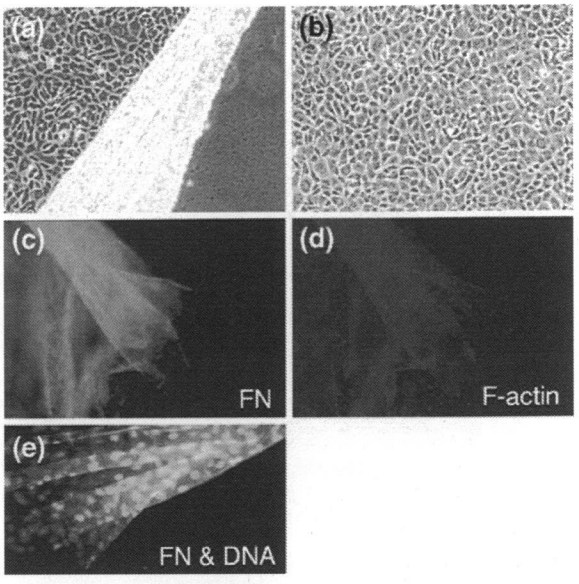

FIGURE 4. Endothelial cell sheet detaching itself from a temperature-responsive surface after low-temperature treatment. ECs were plated on a TCPS surface with or without graft of a temperature-responsive polymer. After cells reached confluency, the culture temperature was decreased to 20 °C, and the cell layer was observed by a phase-contrast microscope. Cells connected with cell–cell junctions detaching themselves as a single sheet from the periphery of TCPS surface grafted with the temperature-responsive polymer (a). Cells on an ungrafted culture surface showed no change (b). Then, detaching and folding cells were fixed and double-stained with anti-FN antibody (c) and rhodamine-phalloidin (d) or with anti-FN antibody and a fluorescent dye for nuclei [(e), superimposed image]. FN matrix was recovered with endothelial cell sheets and no remnant was observed on the surfaces from which the cell sheets detached [the right side in (c, d), the right bottom corner in (e)]. Reproduced with permission from Kushida *et al.*[32] Copyright 1999, John Wiley and Sons.

ACCELERATION OF CELL DETACHMENT FROM TEMPERATURE-RESPONSIVE SURFACES

The rapid recovery of single cell and/or cell sheets is important for maintaining the biological function and viability of recovered cell sheets. In addition, it also contributes the reduction of time necessary for the practical assembly of tissue structures and of patient burden in clinical practice. Although cell sheet detachment can be further accelerated by pipetting or agitation, recovered cell sheets are prone to be friable because of weakened cell–cell junctions. Therefore, spontaneous recovery of cell sheet is strongly required. PIPAAm molecules grafted on a solid interface show temperature-responsive soluble/insoluble changes due to the hydration/dehydration of side groups, resulting in physico-chemical surface property changes, such as a temperature-dependent change in wettability.

Takei *et al.* prepared free end linear PIPAAm-grafted surfaces and multipoint attached PIPAAm surfaces by a coupling reaction between the pendant carboxyl groups of P(IPAAm-*co*-AAc) and aminated glass coverslips.[62,63] The temperature-responsive surface wettability change was investigated using the Wilhelmy plate technique. A large contact angle change was observed for end-grafted PIPAAm surfaces at approximately 24 °C, whereas smaller contact angle changes were observed for P(IPAAm-*co*-AAc)-grafted surfaces over a wide temperature range. The transition temperatures for both surface types were lower than that of PIPAAm in solution, probably due to the influence of the base coating with the polystyrene derivative of dish or base material, as well as the density of the PIPAAm chains. The small contact angle changes of PIPAAm multipoint attached surfaces might be due to the restricted chain conformation of the grafted polymers.

Newly synthesized CIPAAm has a side chain structure that is similar to that of IPAAm and a functional carboxyl group. Therefore, it overcomes the shortcomings of temperature-unsharpness of P(IPAAm-*co*-AAc).[3] In actuality, the P(IPAAm-*co*-CIPAAm) solution shows a steep phase transition in response to temperature, and the LCST is approximately the same as that of PIPAAm solution. Utilizing the advantage of CIPAAm, P(IPAAm-*co*-CIPAAm)-grafted surfaces exhibited a relatively weak hydrophobicity similar to both homopolymer PIPAAm-grafted surfaces as well as commercial ungrafted TCPS surfaces.[14] Cells adhered and spread well on P(IPAAm-*co*-CIPAAm) surfaces at 37 °C in culture. As observed on PIPAAm-grafted surfaces, cells were spontaneously detached themselves from P(IPAAm-*co*-CIPAAm)-grafted surfaces by reducing temperature. Cell detachment was accelerated on the CIPAAm copolymer-grafted surfaces compared to pure PIPAAm surfaces (Fig. 5a). Because hydrophilic-carboxyl-group microenvironment in monomer and polymer is important to accelerate grafted surface hydration below the LCST, detaching cells.

The other challenge of rapid cell sheet recovery was accomplished to use PIPAAm grafted onto porous membranes.[35] Because the rate limiting step of cell sheet recovery is thought to be the hydration of the underlying non-porous PIPAAm-grafted surface. To accelerate the hydration of the hydrophobic PIPAAm segments bound to the cell sheet, the use of a highly water permeable substrate existing in the interface

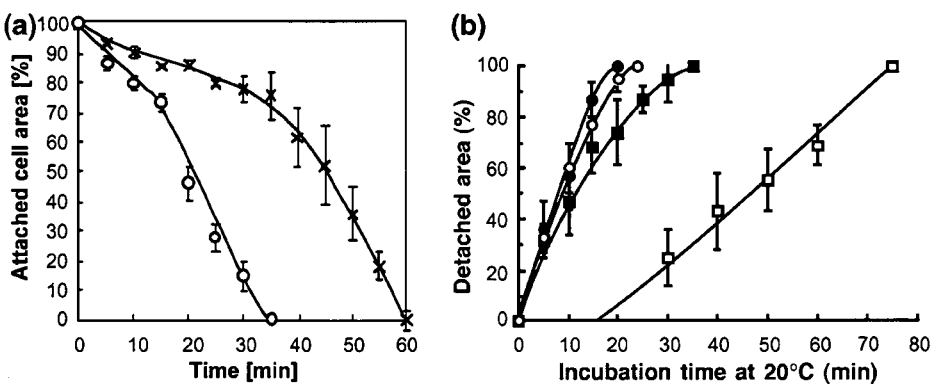

FIGURE 5. (a) Cell sheet recovery from grafted surfaces by reducing culture temperature below the LCST, shown as the percentage of attached cell areas determined for cell sheets recovered from PIPAAm (*the cross*) and P(IPAAm-*co*-CIPAAm)-grafted (CIPAAm 1 mol.% in feed) (*the open circle*) TCPS surfaces as a function of incubation time at 20 °C. (b) Average detached areas for cell sheets recovered from PIPAAm-TCPS (*the open square*), PIPAAm grafted with porous membrane (*the closed square*), PIPAAm grafted with porous membrane containing PEG 0.1% (*the open circle*) and 0.5% (*the closed circle*) as a function of incubation time in culture medium at 20 °C. Adapted from Ebara *et al.*[14] (Copyright 2003, American Chemical Society) and Kwon *et al.*[34] (Copyright 2003, Elsevier).

between the cell sheet and the polymer surface is optimal. Analyses using ATR-FTIR and XPS revealed that PIPAAm was successfully grafted to the surfaces of porous membranes. AFM also supported that PIPAAm-grafted membranes had smoother surfaces than ungrafted controls while retaining their porous structure. The mean roughness of PIPAAm-grafted and -ungrafted porous membrane surfaces determined by digital AFM auto-calculation was 4.40 ± 0.4 and 5.9 ± 0.4 nm, respectively. A grafted porous membrane substrate permits rapid 2-dimensional cell sheet manipulation by facilitating rapid water movement to the interface between the cell sheets and membrane surfaces, producing quick cell sheet release. With these PIPAAm porous membranes, the time needed for complete cell sheet detachment was shortened to be approximately half of the period required with conventional PIPAAm surfaces where non-porous TCPS was used as a substrate. Considering that the amount of PIPAAm grafted onto porous membranes is less than that on PIPAAm surfaces and consequently the amount of hydration force produced for detaching adherent cells is reduced, the observed rapid cell detachment from porous membranes is significant. Cell sheets on PIPAAm-grafted TCPS surfaces initially detach slowly, probably because water requires to hydrate grafted PIPAAm can only penetrate from the cell sheet periphery. Cell sheets on PIPAAm-grafted porous membranes detached more rapidly with the onset of low temperature treatment, suggesting that PIPAAm-grafted porous membranes give a rapid rehydration by water penetration through pores beneath and peripheral to cell sheets at 20 °C.

In addition to the utilization of porous membranes, the co-grafting of a hydrophilic polymer, PEG, with PIPAAm by EB irradiation was also employed to accelerate cell sheet detachment in response to culture temperature alterations.[34] Analyses by ATR-FTIR and XPS revealed that PIPAAm and PEG were successfully grafted to the surfaces of porous membranes. Contact angle of PIPAAm surface grafted with 0.5 wt.% PEG in feed was approximately equivalent to that of PEG non-grafted PIPAAm porous membrane at 37 °C. In contrast, the contact angle of PIPAAm surface grafted with 0.5 wt.% PEG is lower than that of PEG non-grafted PIPAAm porous membrane at 20 °C. This result indicates that (1) grafted PEG chains scarcely exist in the outermost area of the surface at 37 °C, and (2) the interior PEG chains into the surface become more mobile due to hydrophilic PIPAAm chains and exist in the outermost area by reducing temperature, leading to more hydrophilic surface. On the other hand, cells adhered similarly onto both surfaces, hydrophilic domains should be a key factor to the shortened time. The introduction of 0.5 wt.% PEG reduced the time needed for complete cell sheet detachment to nearly the half obtained with temperature-responsive porous membranes (Fig. 5b). Co-grafted PEG chains should accelerate the diffusion of water molecules to PIPAAm surface, resulting in more rapid detachment of single cell and cell sheets, compared to normal PIPAAm-grafted porous membranes.

CELL CULTURE SURFACES ENABLE AFFINITY CONTROL

The interaction of ligands and cell membrane receptors plays multiple important roles for inducing cell spreading, proliferation, differentiation, and signal transduction.[25,69] Surface density and chemical presentation of these synthetic ligands and their effectiveness as surface modification agents in cell culture is correlated to their ability to enhance cell adhesion, particularly, useful for applications in tissue engineering. ECM elaborated by cells on surfaces constitutes a regulator for the cell adhesion process, cell differentiation, and contributes to the mechanical properties of tissue. These regulatory effects of ECM are mediated through transmembrane proteins specialized in cell–substrate adhesion. A peptide sequence Arg-Gly-Asp (RGD) found in fibronectin, type I collagen, and other extracellular matrix proteins has been widely studied as an immobilized cell adhesion ligand specific for integrin-mediated cell adhesion.[39,57] Surface density and the chemical presentation of these synthetic ligands and their effectiveness as surface modification agents in cell culture is correlated to their ability to enhance cell adhesion, particularly, useful for applications in tissue engineering.[21,31,40] PIPAAm-grafted surfaces are modified with RGDS peptides, and the surface swelling, wettabilities, and modulus of the grafted surfaces can be changed by temperature control. Above the LCST of PIPAAm, the grafted polymer chains collapse, and the immobilized peptide is, therefore, exposed to adherent cells. Below the LCST, hydrated polymer chains soften, expand, and swell, followed by a shielding immobilized RGDS from integrin access, a limiting cell–surface attachment tension, and a mechanically disrupting cell–surface contacts.

P(IPAAm-*co*-CIPAAm) has been grafted on TCPS surface via EB irradiation polymerization as mentioned above. Peptides have been immobilized onto the grafted polymer chains via the carboxyl groups in CIPAAm using well-known NHS/EDC chemistry.[12,13] Immobilized RGDS contributed to the enhancement of cell spreading, likely mediated by cell integrins. HUVEC could spread on various P(IPAAm-*co*-CIPAAm) surfaces after 6 and 24 h cultures with or

without serum at 37 °C. By contrast, the spreading improvement was hardly observed on the RGDS modified P(IPAAm-*co*-AAc) surface where peptides were immobilized via another comonomer, AAc, in place of CIPAAm. Detachment rates depended on immobilized cell adhesive peptide densities represented by monomer carboxylate group composition in each feed after reducing temperature. Moreover, the detachment rates were accelerated dramatically by the addition of higher concentrations of RGDS. Low-temperature treatment at 20 °C also promoted cell detachment from RGDS modified P(IPAAm-*co*-CIPAAm) surface, where the detachment rate also decreased with increasing cell adhesive peptide surface content.

Recently, more systematic chemical composition using RGDS modified P(IPAAm-*co*-CIPAAm) systems advances cell attachment and detachment.[11] By co-immobilizing a Pro-His-Ser-Arg-Asn (PHSRN) sequence on intelligent surfaces that enables the stable binding of RGDS to $\alpha 5\beta 1$ integrin, the synergistic roles of the PHSRN sequence have been investigated by studying the time-dependent cell detachment behavior from these surfaces. Notably, PHSRN has been found in fibronectin and is thought to synergistically enhance the cell-adhesive activity of the RGD sequence.[28,38] RGDS-immobilized temperature-responsive polymer-grafted surfaces promote HUVEC adhesion and spreading by their biospecific activity in serum-free media. At temperatures below the grafted polymer's LCST, integrin-RGDS association decreases due to the loss of cell tension and surface anchoring, prompting cells to round and then detach (Fig. 6). Observed "on–off" control of specific integrin-RGDS binding only by temperature regulation is very important for cell function regulation, because cell surface integrins not only bind to cell adhesive ligands in ECM but also serve to produce subsequent cell signal transduction activity. Moreover, this approach facilitates a serum-free cell culture for the safety of clinical applications using cultured cells and noninvasive cell recovery (no enzymes) that help preserving original cell function, both important to the applications of tissue engineering.

J. Vörös and co-workers developed a new cell sheet recovery system using polyelectrolyte film coated on indium tin oxide or titanium oxide.[18] RCOs could be attached and proliferated on the layer consisted of poly(L-lysine)- and ECM-coated indium tin oxide. After electrochemical polarization, cell layers were spontaneously recovered within 10 min. On the other hand, HPDL could be attached and proliferated only

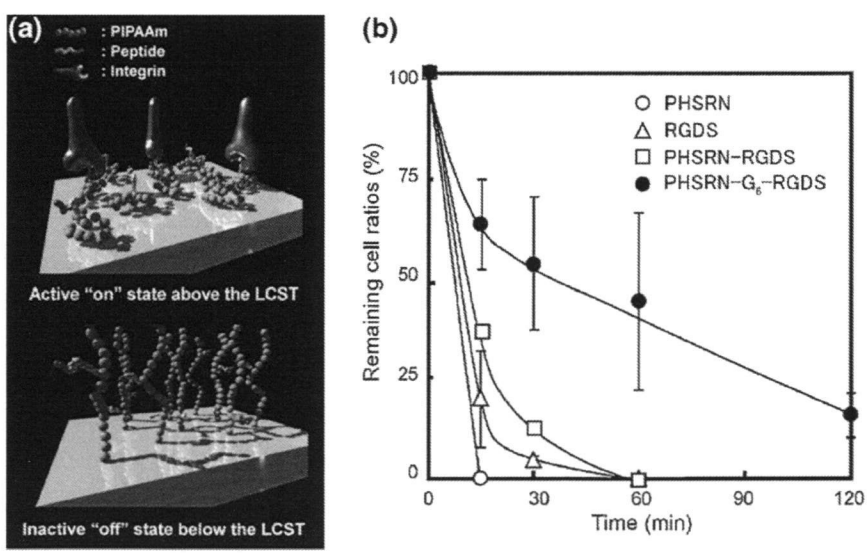

FIGURE 6. (a) Schematic of affinity control between integrin receptors and biomolecule-immobilized temperature-responsive culture surfaces. At temperatures above the LCST, the grafted layer dehydrates and shrinks, thus exposing the immobilized peptides to integrins under cell culture conditions. Upon lowering temperature, the grafted PIPAAm is suddenly hydrated and extends outwards to shield the peptides from integrin access, resulting in decreased binding affinity between integrins and peptides, followed by cell detachment from the surface (b) Detachment profiles for HUVECs seeded on the following peptide-immobilized P(IPAAm-*co*-CIPAAm)-grafted surfaces as a function of time: PHSRN, RGDS, PHSRN–RGDS, and PHSRN-G6-RGDS. The cells have been incubated at 37 °C for 24 h in the absence of FBS, and have been transferred to an incubator equipped with a cooling unit fixed at 20 °C. The results are reported as the percentage of cells remaining on the surfaces. Adapted from and reproduced with permission from Ebara *et al.*[11] Copyright 2008 John Wiley and Sons.

on poly(L-lysine)-*graft*-poly(ethylene glycol) coated indium tin oxide, followed by the cell sheet recovery. These results show that it is possible to induce cell sheet detachment by weakening of the polyelectrolyte interactions between cells and polymer through electrochemical polarization. Polyelectrolyte films have highly tunable properties that can be used for optimizing this new cell sheet engineering method.

CONCLUSION

In this review, we have introduced temperature-responsive intelligent surfaces for cell culture substrates. The creation of these surfaces has been performed using several methodologies, and these surfaces open up a new frontier in the field of cell therapies and tissue engineering. Temperature-responsive surface, involving the precise modification of temperature-responsive polymers, enables us to control cell attachment and detachment in response to temperature. This separation using intelligent chromatography holds promise for the purification of biologically active compounds, pharmaceutical development, and online measurement in clinical practice. Especially, since recovered confluent cell layers as contiguous living cell sheets involves extra cellular matrix in the interior region of the cell layers, they provide novel therapies for difficult-to-treat diseases, with several clinical trials already having been performed. In addition, several other trials related to the preparation of thick and cell-dense tissues and the development of improved temperature-responsive cell culture substrates for the effective preparation of cell sheets have also begun. These developments will ultimately lead to the widespread use of cell sheets in clinical therapy. Thus, the development of these novel intelligent surfaces and their use will facilitate progresses in the fields of medicine and biology. The results could be of significant importance to various biomedical fields.

ACKNOWLEDGMENTS

The present research was financially supported by Formation of Innovation Center for fusion of Advanced Technologies in the Special Coordination Funds for Promoting Science and Technology from the Ministry of Education, Culture, Sports, Science and Technology (MEXT), Japan. The authors are grateful to Dr. N. Ueno (Tokyo Women's Medical University) for her valuable comments and suggestions.

REFERENCES

[1]Akiyama, Y., A. Kikuchi, M. Yamato, and T. Okano. Ultrathin poly(*N*-isopropylacrylamide) grafted layer on polystyrene surfaces for cell adhesion/detachment control. *Langmuir* 20(13):5506–5511, 2004.

[2]Alarco'n, C. H., T. Farhan, V. L. Osborne, W. T. S. Huck, and C. Alexander. Bioadhesion at micro-patterned stimuli-responsive polymer brushes. *J. Mater. Chem.* 15(21):2089–2094, 2005.

[3]Aoyagi, T., M. Ebara, K. Sakai, Y. Sakurai, and T. Okano. Novel bifunctional polymer with reactivity and temperature sensitivity. *J. Biomater. Sci. Polym. Ed.* 11:101–110, 2000.

[4]Barrandon, Y., and H. Green. Cell migration is essential for sustained growth of keratinocyte colonies: the roles of transforming growth factor-α and epidermal growth factor. *Cell* 50(7):1131–1137, 1987.

[5]Canavan, H. E., X. Cheng, D. J. Graham, B. D. Ratner, and D. G. Castner. Cell sheet detachment affects the extracellular matrix: a surface science study comparing thermal liftoff, enzymatic, and mechanical methods. *J. Biomed. Mater. Res. A* 75A(1):1–13, 2005.

[6]Canavan, H. E., X. Cheng, D. J. Graham, B. D. Ratner, and D. G. Castner. Surface characterization of the extracellular matrix remaining after cell detachment from a thermoresponsive polymer. *Langmuir* 21(5):1949–1955, 2004.

[7]Canavan, H. E., D. J. Graham, X. Cheng, B. D. Ratner, and D. G. Castner. Comparison of native extracellular matrix with adsorbed protein films using secondary ion mass spectrometry. *Langmuir* 23(1):50–56, 2007.

[8]Cheng, X., H. E. Canavan, M. J. Stein, J. R. Hull, S. J. Kweskin, M. S. Wagner, G. A. Somorjai, D. G. Castner, and B. D. Ratner. Surface chemical and mechanical properties of plasma-polymerized N-isopropylacrylamide. *Langmuir* 21(17):7833–7841, 2005.

[9]Chung, S. Y. Bladder tissue-engineering: a new practical solution? *Lancet* 367(9518):1215–1216, 2006.

[10]da Silva, R. M. P., J. F. Mano, and R. L. Reis. Smart thermoresponsive coatings and surfaces for tissue engineering: switching cell-material boundaries. *Trends Biotechnol.* 25(12):577–583, 2007.

[11]Ebara, M., M. Yamato, T. Aoyagi, A. Kikuchi, K. Sakai, and T. Okano. A novel approach to observing synergy effects of PHSRN on integrin-RGD binding using intelligent surfaces. *Adv. Mater.* 20(16):3034–3038, 2008.

[12]Ebara, M., M. Yamato, T. Aoyagi, A. Kikuchi, K. Sakai, and T. Okano. Immobilization of cell-adhesive peptides to temperature-responsive surfaces facilitates both serum-free cell adhesion and noninvasive cell harvest. *Tissue Eng.* 10(7–8):1125–1135, 2004.

[13]Ebara, M., M. Yamato, T. Aoyagi, A. Kikuchi, K. Sakai, and T. Okano. Temperature-responsive cell culture surfaces enable "on-off" affinity control between cell integrins and RGDS ligands. *Biomacromolecules* 5(2):505–510, 2004.

[14]Ebara, M., M. Yamato, M. Hirose, T. Aoyagi, A. Kikuchi, K. Sakai, and T. Okano. Copolymerization of 2-carboxyisopropylacrylamide with N-isopropylacrylamide accelerates cell detachment from grafted surfaces by reducing temperature. *Biomacromolecules* 4(2):344–349, 2003.

[15]Fillinger, M. F., E. R. Reinitz, R. A. Schwartz, D. E. Resetarits, A. M. Paskanik, D. Bruch, and C. E. Bredenberg. Graft geometry and venous intimal-medial

hyperplasia in arteriovenous loop grafts. *J. Vasc. Surg.* 11(4):556–566, 1990.
[16]Freed, L. E., G. Vunjak-Novakovic, R. J. Biron, D. B. Eagles, D. C. Lesnoy, S. K. Barlow, and R. Langer. Biodegradable polymer scaffolds for tissue engineering. *Nat. Biotechnol.* 12(7):689–693, 1994.
[17]Fukumori, K., Y. Akiyama, M. Yamato, J. Kobayashi, K. Sakai, and T. Okano. Temperature-responsive glass coverslips with an ultrathin poly (N-isopropylacrylamide) layer. *Acta Biomater.* 5(1):470–476, 2009.
[18]Guillaume-Gentil, O., Y. Akiyama, M. Schuler, C. Tang, M. Textor, M. Yamato, T. Okano, and J. Vörös. Polyelectrolyte coatings with a potential for electronic control and cell sheet engineering. *Adv. Mater.* 20(3):560–565, 2008.
[19]Gupta, S., P. Rajvanshi, R. Sokhi, S. Slehria, A. Yam, A. M. Kerr, and P. Novikoff. Entry and integration of transplanted hepatocytes in rat liver plates occur by disruption of hepatic sinusoidal endothelium. *Hepatology* 29(2):509–519, 1999.
[20]Heskins, M., and J. E. Guillet. Solution properties of poly(N-isopropylacrylamide). *J. Macromol. Sci. A* 2(8):1441–1455, 1968.
[21]Houseman, B. T., J. H. Huh, S. J. Kron, and M. Mrksich. Peptide chips for the quantitative evaluation of protein kinase activity. *Nat. Biotechnol.* 20:270–274, 2002.
[22]Ibusuki, S., Y. Iwamoto, and T. Matsuda. System-engineered cartilage using poly(N-isopropylacrylamide)-grafted gelatin as in situ-formable scaffold: in vivo performance. *Tissue Eng.* 9(6):1133–1142, 2003.
[23]Idota, N., A. Kikuchi, J. Kobayashi, Y. Akiyama, and T. Okano. Thermal modulated interaction of aqueous steroids using polymer-grafted capillaries. *Langmuir* 22(1): 425–430, 2006.
[24]Idota, N., A. Kikuchi, J. Kobayashi, K. Sakai, and T. Okano. Microfluidic valves comprising nanolayered thermoresponsive polymer-grafted capillaries. *Adv. Mater.* 17(22):2723–2727, 2005.
[25]Irvine, D. J., A. M. Mayes, and L. G. Griffith. Nanoscale clustering of RGD peptides at surfaces using comb polymers. 1. Synthesis and characterization of comb thin films. *Biomacromolecules* 2(1):85–94, 2000.
[26]Iwata, T., M. Yamato, H. Tsuchioka, R. Takagi, S. Mukobata, K. Washio, T. Okano, and I. Ishikawa. Periodontal regeneration with multi-layered periodontal ligament-derived cell sheets in a canine model. *Biomaterials* 30(14):2716–2723, 2009.
[27]Jones, D. M., J. R. Smith, W. T. S. Huck, and C. Alexander. Variable adhesion of micropatterned thermoresponsive polymer brushes: AFM investigations of poly(N-isopropylacrylamide) brushes prepared by surface-initiated polymerizations. *Adv. Mater.* 14(16):1130–1134, 2002.
[28]Keselowsky, B. G., D. M. Collard, and A. J. Garcia. Integrin binding specificity regulates biomaterial surface chemistry effects on cell differentiation. *Proc. Natl Acad. Sci. USA* 102(17):5953–5957, 2005.
[29]Kikuchi, A., and T. Okano. Nanostructured designs of biomedical materials: applications of cell sheet engineering to functional regenerative tissues and organs. *J. Controlled Release* 101(1–3):69–84, 2005.
[30]Kobayashi, J., A. Kikuchi, K. Sakai, and T. Okano. Aqueous chromatography utilizing pH-/temperature responsive polymer stationary phases to separate ionic bioactive compounds. *Anal. Chem.* 73(9):2027–2033, 2001.
[31]Koo, L. Y., D. J. Irvine, A. M. Mayes, D. A. Lauffenburger, and L. G. Griffith. Co-regulation of cell adhesion by nanoscale RGD organization and mechanical stimulus. *J. Cell Sci* 115(7):1423–1433, 2002.
[32]Kushida, A., M. Yamato, C. Konno, A. Kikuchi, Y. Sakurai, and T. Okano. Decrease in culture temperature releases monolayer endothelial cell sheets together with deposited fibronectin matrix from temperature-responsive culture surfaces. *J. Biomed. Mater. Res.* 45(4):355–362, 1999.
[33]Kushida, A., M. Yamato, C. Konno, A. Kikuchi, Y. Sakurai, and T. Okano. Temperature-responsive culture dishes allow nonenzymatic harvest of differentiated Madin-Darby canine kidney (MDCK) cell sheets. *J. Biomed. Mater. Res.* 51(2):216–223, 2000.
[34]Kwon, O. H., A. Kikuchi, M. Yamato, and T. Okano. Accelerated cell sheet recovery by co-grafting of PEG with PIPAAm onto porous cell culture membranes. *Biomaterials* 24(7):1223–1232, 2003.
[35]Kwon, O. H., A. Kikuchi, M. Yamato, Y. Sakurai, and T. Okano. Rapid cell sheet detachment from poly(N-isopropylacrylamide)-grafted porous cell culture membranes. *J. Biomed. Mater. Res.* 50(1):82–89, 2000.
[36]Langer, R., and J. Vacanti. Tissue engineering. *Science* 260(5110):920–926, 1993.
[37]Langer, R., and J. Vacanti. Tissue engineering: the challenges ahead. *Sci. Am.* 280(4):86–89, 1999.
[38]Leahy, D. J., I. Aukhil, and H. P. Erickson. 2 Dimensional crystal structure of a four-domain segment of human fibronectin encompassing the RGD loop and synergy region. *Cell* 84(1):155–164, 1996.
[39]Leahy, D. J., W. A. Hendrickson, I. Aukhil, and H. P. Erickson. Structure of a fibronectin type III domain from tenascin phased by MAD analysis of the selenomethionyl protein. *Science* 258(5084):987–991, 1992.
[40]Massia, S. P., and J. A. Hubbell. An RGD spacing of 440 nm is sufficient for integrin alpha V beta 3-mediated fibroblast spreading and 140 nm for focal contact and stress fiber formation. *J. Cell Biol.* 114(5):1089–1100, 1991.
[41]Matsuda, T. Poly(N-isopropylacrylamide)-grafted gelatin as a thermoresponsive cell-adhesive, mold-releasable material for shape-engineered tissues. *J. Biomater. Sci. Polym. Ed.* 15:947–955, 2004.
[42]Memon, I. A., Y. Sawa, N. Fukushima, G. Matsumiya, S. Miyagawa, S. Taketani, S. K. Sakakida, H. Kondoh, A. N. Aleshin, T. Shimizu, T. Okano, and H. Matsuda. Repair of impaired myocardium by means of implantation of engineered autologous myoblast sheets. *J. Thorac. Cardiovasc. Surg.* 130(5):1333–1341, 2005.
[43]Mizutani, A., A. Kikuchi, M. Yamato, H. Kanazawa, and T. Okano. Preparation of thermoresponsive polymer brush surfaces and their interaction with cells. *Biomaterials* 29(13):2073–2081, 2008.
[44]Nagase, K., J. Kobayashi, A. Kikuchi, Y. Akiyama, H. Kanazawa, and T. Okano. Interfacial property modulation of thermoresponsive polymer brush surfaces and their interaction with biomolecules. *Langmuir* 23(18):9409–9415, 2007.
[45]Nagase, K., J. Kobayashi, A. Kikuchi, Y. Akiyama, H. Kanazawa, and T. Okano. Effects of graft densities and chain lengths on separation of bioactive compounds by nanolayered thermoresponsive polymer brush surfaces. *Langmuir* 24(2):511–517, 2008.
[46]Nakayama, M., J. E. Chung, T. Miyazaki, M. Yokoyama, K. Sakai, and T. Okano. Thermal modulation of intracellular

drug distribution using thermoresponsive polymeric micelles. *React. Funct. Polym.* 67(11):1398–1407, 2007.

[47]Nakayama, M., and T. Okano. Polymer terminal group effects on properties of thermoresponsive polymeric micelles with controlled outer-shell chain lengths. *Biomacromolecules* 6(4):2320–2327, 2005.

[48]Nishida, K., M. Yamato, Y. Hayashida, K. Watanabe, N. Maeda, H. Watanabe, K. Yamamoto, S. Nagai, A. Kikuchi, Y. Tano, and T. Okano. Functional bioengineered corneal epithelial sheet grafts from corneal stem cells expanded ex vivo on a temperature-responsive cell culture surface. *Transplantation* 77(3):379–385, 2004.

[49]Nishida, K., M. Yamato, Y. Hayashida, K. Watanabe, K. Yamamoto, E. Adachi, S. Nagai, A. Kikuchi, N. Maeda, H. Watanabe, T. Okano, and Y. Tano. Corneal reconstruction with tissue-engineered cell sheets composed of autologous oral mucosal epithelium. *N. Engl. J. Med.* 351(12):1187–1196, 2004.

[50]Ohashi, K., T. Yokoyama, M. Yamato, H. Kuge, H. Kanehiro, M. Tsutsumi, T. Amanuma, H. Iwata, J. Yang, T. Okano, and Y. Nakajima. Engineering functional two- and three-dimensional liver systems in vivo using hepatic tissue sheets. *Nat. Med.* 13(7):880–885, 2007.

[51]Ohki, T., M. Yamato, D. Murakami, R. Takagi, J. Yang, H. Namiki, T. Okano, and K. Takasaki. Treatment of oesophageal ulcerations using endoscopic transplantation of tissue-engineered autologous oral mucosal epithelial cell sheets in a canine model. *Gut* 55(12):1704–1710, 2006.

[52]Ohya, S., S. Kidoaki, and T. Matsuda. Poly(N-isopropylacrylamide) (PNIPAM)-grafted gelatin hydrogel surfaces: interrelationship between microscopic structure and mechanical property of surface regions and cell adhesiveness. *Biomaterials* 26(16):3105, 2005.

[53]Ohya, S., and T. Matsuda. Poly (N-isopropylacrylamide) (PNIPAM)-grafted gelatin as thermoresponsive three-dimensional artificial extracellular matrix: molecular and formulation parameters vs. cell proliferation potential. *J. Biomater. Sci. Polym. Ed.* 16:809–827, 2005.

[54]Okano, T., N. Yamada, M. Okuhara, H. Sakai, and Y. Sakurai. Mechanism of cell detachment from temperature-modulated, hydrophilic-hydrophobic polymer surfaces. *Biomaterials* 16(4):297–303, 1995.

[55]Okano, T., N. Yamada, H. Sakai, and Y. Sakurai. A novel recovery system for cultured cells using plasma-treated polystyrene dishes grafted with poly(N-isopropylacrylamide). *J. Biomed. Mater. Res.* 27(10):1243–1251, 1993.

[56]Pan, Y. V., R. A. Wesley, R. Luginbuhl, D. D. Denton, and B. D. Ratner. Plasma polymerized N-isopropylacrylamide: synthesis and characterization of a smart thermally responsive coating. *Biomacromolecules* 2(1):32–36, 2000.

[57]Pytela, R., M. D. Pierschbacher, M. H. Ginsberg, E. F. Plow, and E. Ruoslahti. Platelet membrane glycoprotein IIb/IIIa: member of a family of Arg-Gly-Asp-specific adhesion receptors. *Science* 231(4745):1559–1562, 1986.

[58]Shimizu, T., H. Sekine, Y. Isoi, M. Yamato, A. Kikuchi, and T. Okano. Long-term survival and growth of pulsatile myocardial tissue grafts engineered by the layering of cardiomyocyte sheets. *Tissue Eng.* 12(3):499–507, 2006.

[59]Shimizu, T., H. Sekine, J. Yang, Y. Isoi, M. Yamato, A. Kikuchi, E. Kobayashi, and T. Okano. Polysurgery of cell sheet grafts overcomes diffusion limits to produce thick, vascularized myocardial tissues. *Faseb J.* 20(1):708–710, 2006.

[60]Shimizu, T., M. Yamato, Y. Isoi, T. Akutsu, T. Setomaru, K. Abe, A. Kikuchi, M. Umezu, and T. Okano. Fabrication of pulsatile cardiac tissue grafts using a novel 3-dimensional cell sheet manipulation technique and temperature-responsive cell culture surfaces. *Circ. Res.* 90(3): E40–E48, 2002.

[61]Shimizu, T., M. Yamato, A. Kikuchi, and T. Okano. Cell sheet engineering for myocardial tissue reconstruction. *Biomaterials* 24(13):2309–2316, 2003.

[62]Takei, Y. G., T. Aoki, K. Sanui, N. Ogata, T. Okano, and Y. Sakurai. Temperature-responsive bioconjugates. 1. Synthesis of temperature-responsive oligomers with reactive end groups and their coupling to biomolecules. *Bioconjug. Chem.* 4(1):42–46, 1993.

[63]Takei, Y. G., T. Aoki, K. Sanui, N. Ogata, Y. Sakurai, and T. Okano. Dynamic contact angle measurement of temperature-responsive surface properties for poly(N-isopropylacrylamide) grafted surfaces. *Macromolecules* 27(21): 6163–6166, 1994.

[64]Takezawa, T., Y. Mori, and K. Yoshizato. Cell culture on a thermo-responsive polymer surface. *Nat. Biotechnol.* 8(9): 854–856, 1990.

[65]Takezawa, T., M. Yamazaki, Y. Mori, T. Yonaha, and K. Yoshizato. Morphological and immuno-cytochemical characterization of a hetero-spheroid composed of fibroblasts and hepatocytes. *J. Cell Sci.* 101(3):495–501, 1992.

[66]Todaro, G. J., and H. Green. Quantitative studies of the growth of mouse embryo cells in culture and their development into established lines. *J. Cell Biol.* 17(2):299–313, 1963.

[67]von Recum, H., S. W. Kim, A. Kikuchi, M. Okuhara, Y. Sakurai, and T. Okano. Novel thermally reversible hydrogel as detachable cell culture substrate. *J. Biomed. Mater. Res.* 40(4):631–639, 1998.

[68]von Recum, H., A. Kikuchi, M. Yamato, Y. Sakurai, T. Okano, and S. W. Kim. Growth factor and matrix molecules preserve cell function on thermally responsive culture surfaces. *Tissue Eng.* 5(3):251–265, 1999.

[69]Whitesides, G. M., J. P. Mathias, and C. T. Seto. Molecular self-assembly and nanochemistry: a chemical strategy for the synthesis of nanostructures. *Science* 254(5036): 1312–1319, 1991.

[70]Yamada, N., T. Okano, K. Sakai, F. Karikusa, Y. Sawasaki, and Y. Sakurai. Thermo-responsive polymeric surfaces; control of attachment and detachment of cultured cells. *Makromol. Rapid Commun.* 11(11):571–576, 1990.

[71]Yamato, M., C. Konno, A. Kushida, M. Hirose, M. Utsumi, A. Kikuchi, and T. Okano. Release of adsorbed fibronectin from temperature-responsive culture surfaces requires cellular activity. *Biomaterials* 21(10):981–986, 2000.

[72]Yamato, M., M. Okuhara, F. Karikusa, A. Kikuchi, Y. Sakurai, and T. Okano. Signal transduction and cytoskeletal reorganization are required for cell detachment from cell culture surfaces grafted with a temperature-responsive polymer. *J. Biomed. Mater. Res.* 44(1):44–52, 1999.

[73]Yang, J., M. Yamato, T. Shimizu, H. Sekine, K. Ohashi, M. Kanzaki, T. Ohki, K. Nishida, and T. Okano. Reconstruction of functional tissues with cell sheet engineering. *Biomaterials* 28(34):5033–5043, 2007.

[74]Yoshida, R., K. Uchida, Y. Kaneko, K. Sakai, A. Kikuchi, Y. Sakurai, and T. Okano. Comb-type grafted hydrogels with rapid deswelling response to temperature changes. *Nature* 374(6519):240–242, 1995.

ELSEVIER

Experimental Hematology

Experimental Hematology 2009;37:334–345

Increase of hematopoietic progenitor and suppression of endothelial gene expression by Runx1 expression during in vitro ES differentiation

Eiko Sakai[a], Kenji Kitajima[a], Ayuko Sato[a,b], and Toru Nakano[a]

[a]*Department of Pathology, School of Medicine and Frontier Biosciences, Osaka University, Osaka, Japan;* [b]*Department of Pathology, Hyogo College of Medicine, Hyogo, Japan*

(Received 1 July 2008; revised 12 November 2008; accepted 13 November 2008)

Objective. **Runx1 is essential for both the establishment of hematopoiesis during development and maintenance of adult hematopoiesis. To reveal the roles of Runx1, we examined how and when Runx1 functions during development of hematopoiesis, and revealed the genes controlled by Runx1.**

Materials and Methods. **A combined in vitro approach involving in vitro hematopoietic differentiation of embryonic stem cells and conditional gene expression of Runx1 was utilized for this study. Then we analyzed the effects of Runx1 on the differentiation and proliferation of hematopoietic cells and carried out DNA microarray analysis.**

Results. **Pulse expression of Runx1 prior to the emergence of hematopoietic cells caused immature hematopoietic cell increase but did not have any effects on the induction of hemogenic cells. During this process, the mRNA level of several endothelial cell-specific genes was downregulated.**

Conclusion. **Runx1 expression play important roles on the proliferation of emerging immature hematopoietic progenitors or the transition process from endothelial to hematopoietic cells presumably by suppressing the genes related to endothelial phenotype.** © **2009 ISEH - Society for Hematology and Stem Cells. Published by Elsevier Inc.**

Hematopoiesis originates from two distinct waves during two embryonic phases. The first is a brief primitive wave that occurs in the yolk sac very early during embryogenesis, and which generates mainly erythrocytes. The second is definitive hematopoiesis, which generates hematopoietic progenitor cells (HPCs) and long-term repopulating hematopoietic stem cells, which are capable of reconstituting the entire adult hematopoietic system. It has been suggested that hematopoietic cells differentiate from the mesoderm via a common endothelial and hematopoietic precursor, the hemangioblast, or hemogenic endothelium [1].

Lineage tracing in chickens and mice has revealed that the hematopoietic cells emerge from the hemogenic endothelium [2,3]. Vascular endothelium−cadherin$^+$ endothelial cells isolated from mouse embryos have been shown to generate HPCs when cultured in vitro [4], suggesting that at least a subpopulation of the definitive HPCs are generated directly from endothelial cells. The hematopoietic differentiation of embryonic stem (ES) cells has been extensively investigated in vitro. The initial stages of ES cell differentiation have been studied in detail, and the mesodermal and hematopoietic precursor stages that arise during this process are well-defined [5–7]. During embryoid-body formation [5], mesodermal cells appear that differentiate into blast colony-forming cells and putative hemangioblasts [1,8] around days 2.5 to 3.5 and 3.5 to 4.5, respectively. The first definitive HPC colonies can be detected around day 4.5 in cultures grown on OP9 stromal cells [9].

Runx1 encodes the DNA-binding subunit of a heterodimeric transcription factor, core-binding factor (CBF)/PEBP2 [10,11]. While the other subunit, CBF subunit b stabilizes the complex formation of Runx1 and DNA [12,13], Runx1 bears the transcriptional regulatory function of CBF/PEBP2 through the binding with transcriptional

Offprint requests to: Toru Nakano, M.D., Ph.D., Department of Pathology, School of Medicine and Frontier Biosciences, Osaka University, Yamadaok 2-2, Osaka, Japan; E-mail: esakai@patho.med.osaka-u.ac.jp; tnakano@patho.med.osaka-u.ac.jp

0301-472X/09 $–see front matter.
doi: 10.1016/j.exphem.2008.11.007

activators and repressors [14–16]. Homozygous null *Runx1* mutants still exhibit primitive hematopoiesis in the yolk sac [17,18]; however, they do not develop definitive hematopoietic cells, indicating that Runx1 plays a critical role in the initiation of definitive hematopoiesis [17,18]. Nevertheless, it is unclear how the function of Runx1 is integrated into the process.

In vitro ES cell differentiation with tetracycline-based conditional gene expression is a powerful tool for analyzing the specific functions of genes at distinct stages of hematopoietic development and differentiation [19,20]. Previous studies using mouse ES cells cocultured on OP9 stromal cells revealed that hematopoietic differentiation from primitive to definitive hematopoiesis occurs in a synchronous manner [21,22]. Here, using the OP9 system with conditional gene expression, we show that conditional Runx1 expression induces the increase of immature hematopoietic progenitor. Moreover, we identified a number of genes that are regulated by Runx1, some of which are related to endothelial cells. Thus, using a single experimental system, we identified Runx1 as the driving force behind the increase of immature hematopoietic cells, as well as the gene regulation in transition from endothelial to hematopoietic cells.

Material and methods

Cell culture

The E14Tg2a ES clone P2-1 and its derivatives were maintained as described previously [19] and ES clones that conditionally express cRunx1 and dominant negative form of Runx1 (DNRunx1) on tetracycline induction were established using a protocol described previously [19,20]. Briefly, mouse *Runx1* cDNA fragments encoding residues 51–451 or 51–185 were amplified from the full-length mouse *Runx1* cDNA (encoding residues 1–451) and its splicing variant (encoding residues 1–185) by polymerase chain reaction (PCR) and each fragment was inserted into the *EcoRI* site of pUHD10-3.IRES-EGFP to create cRunx1- and DNRunx1-expressing vectors, respectively. Each construct was then linearized and cotransfected with pPGKneo into P2-1 ES cells. The clones in which enhanced green fluorescent protein (EGFP) expression was tightly regulated were selected for use in our experiments. Our in vitro culture system for differentiation of hematopoietic cells from ES cells on OP9 stromal cells was described previously [21,22]. Briefly, 6×10^4 ES cells per six-well plate were seeded onto an OP9 cell layer, and the cells were collected by dissociation on day 4 or 5 and replated onto fresh OP9 cells. Human erythropoietin (2 U/mL), human thrombopoietin (10 ng/mL), human macrophage colony-stimulation factor (10 ng/mL), and human FMS-like tyrosine kinase 3 ligand (5 ng/mL) ((R & D Systems, Minneapolis, MN, USA) were added to the culture on day 5 as necessary. Erythropoietin was kindly provided by Kirin Brewery Co. (Tokyo, Japan), while thrombopoietin and macrophage colony-stimulation factor were kind gifts of the Morinaga Milk Co. (Tokyo, Japan). A colony-formation assay was carried out using the methylcellulose culture medium Methocult M3232 (StemCell Technology, Vancouver, Canada) as described previously [20] and the colonies were analyzed 8 days later.

Assay for HPC-producing cells

Induction of differentiation was carried out as described here, and the cells were harvested by treatment with trypsin at day 4 or day 5, replated onto fresh OP9 feeder layer at the density of 10^3 or 5×10^2 per 96-well plate, respectively. At day 12, all wells were examined the presence of hematopoietic colonies consisting with round-shape cells loosely attached on the feeder layer under microscope. Three plates were examined for each density and the data of the density at which the number of HPC-positive wells was <21 per plate was used for the analysis, because the positive wells were assumed to contain HPC from single HPC-producing cell.

Flow cytometry

Primary antibodies used were biotin-anti–Flk1 (eBioscience, San Diego, CA, USA), biotin-anti–Ter119 (a gift from Dr. Kina, Kyoto University, Japan), biotin-anti–Mac1, biotin-anti–glycoprotein V, phycoerythrin (PE)-anti–CD71, PE-anti–c-kit, unlabeled anti-CD41 (BD Pharmingen, San Diego, CA, USA). The unlabeled and biotinylated antibodies were visualized using anti-rat Igκ and cytochrome-conjugated streptavidin (BD Pharmingen), respectively. Cells were stained with antibodies as described previously [20], then analyzed and sorted using a FACSCalibur flow cytometer (Becton Dickinson, Franklin Lakes, NJ, USA).

Western blotting

Western blotting was performed as described previously [20]. The blotted membranes were probed with rabbit polyclonal anti-Runt homology domain of mouse Runx1 (residues 50–177: AML1/RHD Ab-2; Oncogene Research Products, San Diego, CA, USA) and reprobed with mouse monoclonal anti–β-actin antibody (AC-15; Sigma, St Louis, MO, USA). Horseradish peroxidase–conjugated anti-rabbit and anti-mouse IgG antibodies (Zymed, San Francisco, CA, USA) were used as secondary antibodies. Detection was performed using an ECL detection kit (Amersham Pharmacia, Buckinghamshire, UK).

Reverse transcription PCR

Total RNA was purified using an RNeasy Mini Kit (Qiagen, Valencia, CA, USA), and cDNA was synthesized from 1 μg RNA using a ThermoScript RT-PCR system (Gibco BRL, Rockville, MD, USA). The primer sequences used for detection of the *gapdh* cDNAs were described previously [22]. The remaining primer sequences were as follows:

Endothelin-1 sense: 5′-CTGTTCGTGACTTTCCAAG GAGCTC -3′;

Endothelin-1 anti-sense: 5′-ATGTGCTCGGTTGTGCGT CAACTTC-3′;

Endomucin-1 sense: 5′-TGAGAGGAATCCTTCCCTGC CTTAC-3′;

Endomucin-1 anti-sense: 5′-TTGTTCTGGGAACCTGG TAGCGTTG-3′;

ICAM-2 sense: 5′-ATAGACTCCACAGACCCCACA GAC-3′;

ICAM-2 anti-sense: 5′-ATTCTTCAGGGTCTCTCTGC CACG-3′;

Flk1 sense: 5′-CGTGGATCTGAAAAGACGCTTG GAC-3′;

Flk1 anti-sense: 5′-TTTCTGGGGTAGTGTAGTCAG GAGC-3′;

β-actin sense: 5′-ATGAAGATCCTGACCGAGCG

β-actin anti-sense: 3′-TACTTGCGCTCAGGAGGAGC

runx1 sense: 5′-CTTGTTGTGATGCGTATCCCCGTAG

runx1 anti-sense: 3′-GGGTTCTCGGGGGCCGTCCA CTGTG

All sequences were of murine origin.

DNA microarray analysis

The ES cells were first induced to differentiate on OP9 cells. They were then harvested on day 4 and stained with biotin-anti−Flk1, followed by treatment with an anti-biotin MultiSort Kit (Miltenyi Biotech, Auburn, CA, USA) to isolate Flk1$^+$ cells using AutoMACS (Miltenyi Biotech). The isolated Flk1$^+$ cells were stained with PE-anti−c-kit, followed by treatment with anti-PE Micro Beads, and the Flk1$^+$c-kit$^+$ cells were purified by Auto-MACS. These cells were subsequently reseeded on a new OP9 layer and cRunx1 expression was induced. After 18 hours, total RNA was isolated using an RNeasy Mini Kit and polyA$^+$ RNA was purified using an mRNA purification kit (Amersham Pharmacia). Double-stranded cDNA was synthesized from 1 μg mRNA using the SuperScript Choice System (Invitrogen, Carlsbad, CA, USA) with a T7-(dT)24 primer, then used to prepare biotin-labeled cRNA by in vitro transcription using T7 RNA polymerase in the presence of biotinylated ribonucleotides according to manufacturer's instructions (Enzo Diagnostics, Farmingdale, NY, USA). The cRNA was then purified using an RNeasy Kit (Qiagen), fragmented, and hybridized to Affymetrix Murine Genome U74 Av2 microarray chips according to manufacturer's instructions (Affymetrix, Santa Clara, CA, US). Hybridized chips were stained, washed, and scanned with a GeneArray Scanner (Affymetrix).

Results

Conditional expression of the functional and dominant negative forms of Runx1 in an in vitro hematopoietic cell differentiation system

We generated tetracycline-regulatable transgenes of Runx1 derivatives in ES cells (Fig. 1A) and applied them to an in

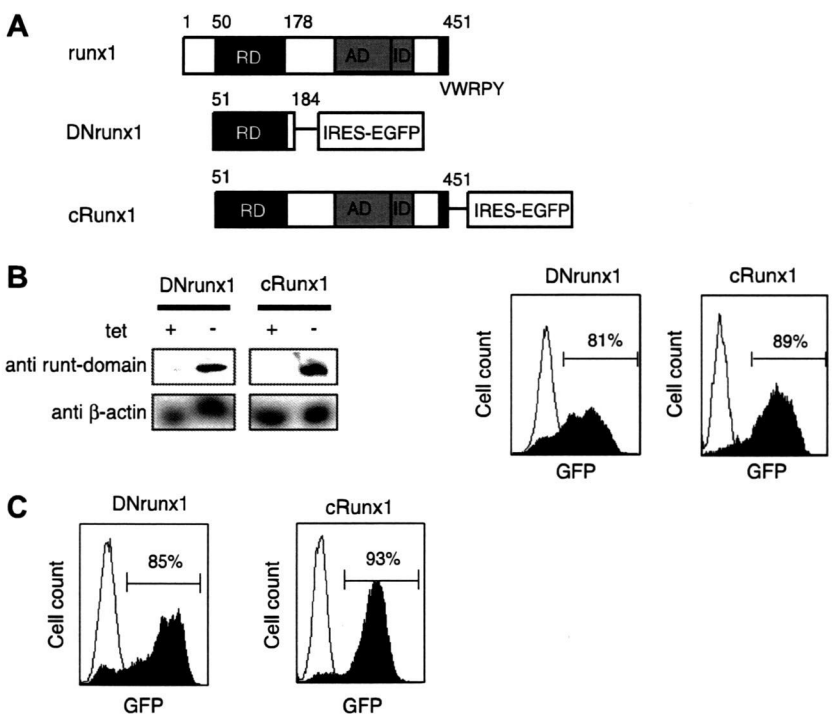

Figure 1. Establishment of a Tet-regulated inducible overexpression system for *Runx1*. (**A**) Schematic of Runx1 and its derivatives. The dominant negative form (DNRunx1) carries the Runt domain, but not the C-terminal regulatory region or the N-terminal region. The functional form (cRunx1) lacks the N-terminus of the Runt domain. Both are bicistronically expressed with enhanced green fluorescent protein (EGFP) under a Tet-regulated promoter that is activated in the absence of tetracycline. RD, AD, ID, and VWRPY indicate the Runt domain, activation domain, inhibitory domain, and VWRPY motif, respectively. (**B**) Controlled expression of DNRunx1, cRunx1, and EGFP. Undifferentiated ES cells maintained in the presence of tetracycline were induced to express either DNRunx1 or cRunx1 by the withdrawal of tetracycline for 24 hours. The levels of cRunx1 protein and EGFP fluorescence were analyzed by Western blotting (left) and fluorescein-activated cell sorting (FACS) (right), respectively. Dotted lines indicate the level of EGFP in the control culture, where tetracycline was in the medium. (**C**) Controlled expression of EGFP after differentiation on OP9 cells. ES cells maintained in the presence of tetracycline were induced to differentiate by culturing on OP9 stromal cells. Tetracycline was withdrawn from day 4 to day 5 to induce either DNRunx1 or cRunx1. EGFP expression was analyzed by FACS on day 5.

vitro hematopoietic cell differentiation system using OP9 stromal cells. We constructed an effecter molecule containing both DNA binding and transcriptional regulatory regions but not an N-terminal portion, designated cRunx1, as a transcriptionally effective molecule. This form was previously shown to activate transcription at a level comparable to that by the full-length isoform Runx1b [23]. We also used a DNRunx1 that carries only the Runt homology domain, which contains the regions responsible for DNA binding, heterodimerization, and nuclear localization, but not for transcriptional regulation [23,24].

The cDNAs of *cRunx1* and *DNRunx1* were cloned into a vector containing a tetracycline-regulatory element and stably transformed the ES cell line E14Tg2a2.1, which expresses a tetracycline-dependent transactivator [19]. Induction of *cRunx1* and *DNRunx1* by the withdrawal of tetracycline was monitored by EGFP expression. Two ES cell lines in which GFP was expressed in a tetracycline-dependent manner were selected. We used representative clones in which *cRunx1* and *DNRunx1* were efficiently induced because all of the clones examined showed similar results (data not shown). After the removal of tetracycline, 89% and 81% of the *cRunx1* and *DNRunx1* clones were both GFP-positive, respectively, and the proteins were also efficiently induced (Fig. 1B). Expression of GFP was also monitored after transferring the cells to OP9 stromal cells for hematopoietic differentiation. When tetracycline was eliminated from the media 4 days after the transfer, GFP was successfully expressed at a high frequency (85% and 93%, respectively) within 24 hours (Fig. 1C).

Runx1 increases the mature blood cells when expressed at an early stage of hematopoiesis

Runx1-deficient mice have complete defects in definitive hematopoiesis, indicating the critical role this protein plays in the initial step of definitive hematopoiesis. To verify that our experimental system could be used to monitor some stages of the development of definitive hematopoiesis, we inhibited endogenous Runx1 function via conditional DNRunx1 expression. The level of endogenous *Runx1* mRNA was detectable but very low on day 2 of differentiation; however, it began to increase on day 3 and continued for the next 6 to 7 days before declining (Fig. 2A). Some low-level expression of runx1 was also observed in the undifferentiated ES cells (day 0) as reported previously [25]. When DNRunx1 expression was induced during the transition from mesodermal to hematopoietic cells (days 2–5 of differentiation), the number of cells present on day 12 was decreased 2.6-fold, as expected (Fig. 2B). A similar reduction in cell number was observed following DNRunx1 expression on days 3 to 5 and days 4 to 5. These results indicate that runx1 expression at these periods contributed to hematopoietic cell production in this system.

Our results also indicate that days 4 and 5 are the critical period for endogenous Runx1 function in the production of hematopoietic cells. Forced expression of cRunx1 between days 4 and 5 significantly enhanced hematopoiesis (Fig. 2C). Interestingly, this effect was opposite to that of DNRunx1 pulse expression during the same period. cRunx1 protein expression was detectable until day 5, after which it declined rapidly and became undetectable by day 6 (Fig. 2D). The strictly controlled expression of the cRunx1 protein in this system shows that a limited duration of *cRunx1* expression, as short as 1 day, is sufficient to demonstrate its critical role in the observed effect of runx1.

Using the OP9 differentiation method, definitive progenitors first become detectable between days 4.5 and 5, and thereafter they differentiate to committed and more mature HPCs [9]. Expression of cRunx1 on days 4 and 5 enhanced the production of c-kit$^+$CD41$^+$ population at day 6 and this population included immature hematopoietic progenitors (Fig. 2E). cRunx1 expression also enhanced the production of erythrocytes, megakaryocytes, and macrophages in the presence of erythropoietin, thrombopoietin, and macrophage colony-stimulation factor, respectively, to a similar extent. Notably, B-lymphocyte production was also enhanced in the presence of FMS-like tyrosine kinase 3 ligand (Fig. 2F). The cells cultured with these cytokines were analyzed for the surface marker expression (Fig. 2G). The hematopoietic cells derived from cRunx1-induced cells exhibited the similar expression patterns to the control. These data suggest that cRunx1 expression during this period results in an increase in various hematopoietic lineages, including myeloid and lymphoid progenitors, and/or their common progenitors.

cRunx1 enhances hematopoietic progenitor development but does not expand the hemogenic cell pool

The target process of cRunx1 function was analyzed as follows. When nonadherent and loosely attached hematopoietic cells were collected on day 6 after conditional cRunx1 expression on days 4 and 5 and transferred into methylcellulose media, an increased number of mixed colonies were observed (Fig. 3A). This confirms that cRunx1 increases the number of immature HPCs by day 6. In the course of HPC differentiation, a small proportion of Flk1$^+$ mesodermal cells begins to express Runx1, and these cells are referred to as the hemogenic population [1]. Therefore, the increased number of HPCs is attributable to increase of the hemogenic cells, either by proliferation or conversion from nonhemogenic cells, and/or the proliferation of hematopoietic progenitors.

To investigate this, cRunx1 was expressed on days 4 and 5, the cells were dissociated by trypsinization on day 5 and transferred to a fresh OP9 cell layer, and the number of HPC-producing cells was examined on day 9 (Fig. 3B). Because the number of HPC-producing cells (i.e., hemogenic cells) was limited under these experimental conditions, even a slight increase in the number of hemogenic

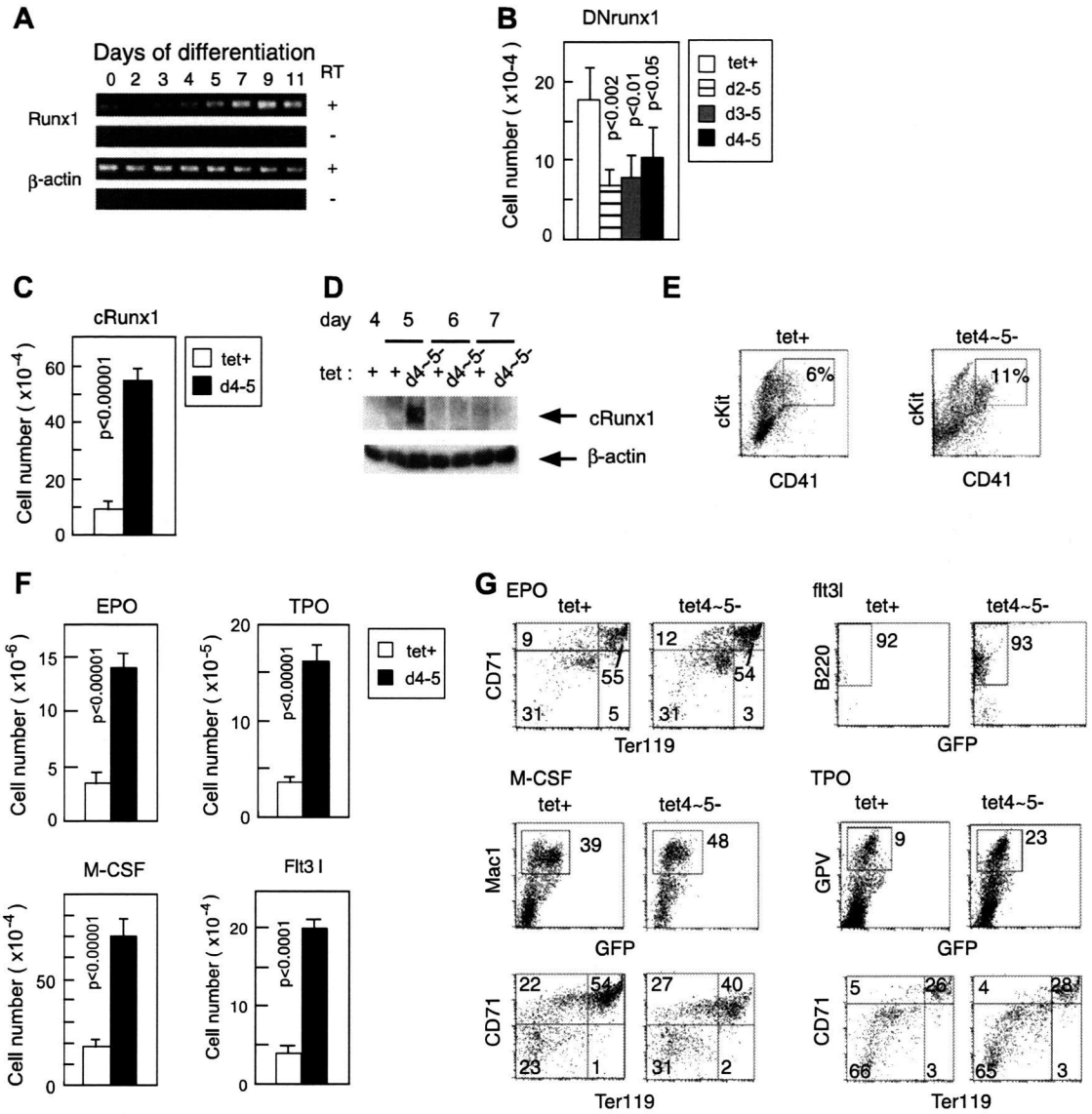

Figure 2. Enhanced hematopoiesis by functional Runx1 expression in the early differentiation stage. (**A**) Expression of endogenous runx1 during embryonic stem (ES) differentiation. mRNA was prepared at the indicated day of differentiation and analyzed by reverse transcription polymerase chain reaction. (**B**,**C**) Number of cells after conditional expression of DNRunx1 and cRunx1. ES cells were differentiated on OP9 stromal cells. DNRunx1 (**B**) or cRunx1 (**C**) expression was induced for the indicated period by the withdrawal of tetracycline during the course of differentiation. The cells were harvested on day 12 and counted (n = 6). (**D**) Expression of cRunx1. cRunx1 expression was induced by the withdrawal of tetracycline from day 4 to day 5 of differentiation on OP9 cells. The cells were harvested on the indicated day and the protein level was examined by Western blot analysis. (**E**) Increase of c-kit$^+$CD41$^+$ population by cRunx1 expression. The cRunx1-induced and control cells were stained with the anti−c-kit and CD41 antibodies and analyzed by fluorescein-activated cell sorting (FACS) at day 6. (**F**) Number of cells after cRunx1 expression in the presence of erythropoietin (EPO), thrombopoietin (TPO), macrophage colony-stimulation factor (M-CSF), or FMS-like tyrosine kinase 3 (Flt-3) ligand. cRunx1-inducible ES cells were differentiated on OP9 cells in the presence of tetracycline for 4 days. Tetracycline was removed from the media between days 4 and 5 and the cells were cultured afterwards in the presence of tetracycline and the indicated cytokines. Cells were counted on day 17 for Flt-3 ligand (n = 5) and on day 12 for the other cytokines (n = 6). (**G**) The cells in (**F**) were stained with erythroid marker CD71 and Ter119, myeloid marker Mac-1, megakaryocytic marker GPV and B-cell marker B220 in the presence of EPO, M-CSF, TPO, and Flt3 ligand, respectively, and analyzed by FACS.

cells should result in an increase in the number of HPC-containing wells. However, cRunx1 expression did not increase the number of wells containing HPCs (Fig. 3B), demonstrating that cRunx1 did not induce increase of hemogenic cell. A similar experiment, in which the order of dissociation of the cells was changed, confirmed this result. In that experiment, the cells were trypsinized on day 4, transferred to a new OP9 cell layer, cRunx1 was expressed on days 4 and 5, and the same analysis was performed. Here again, no increase in the number of

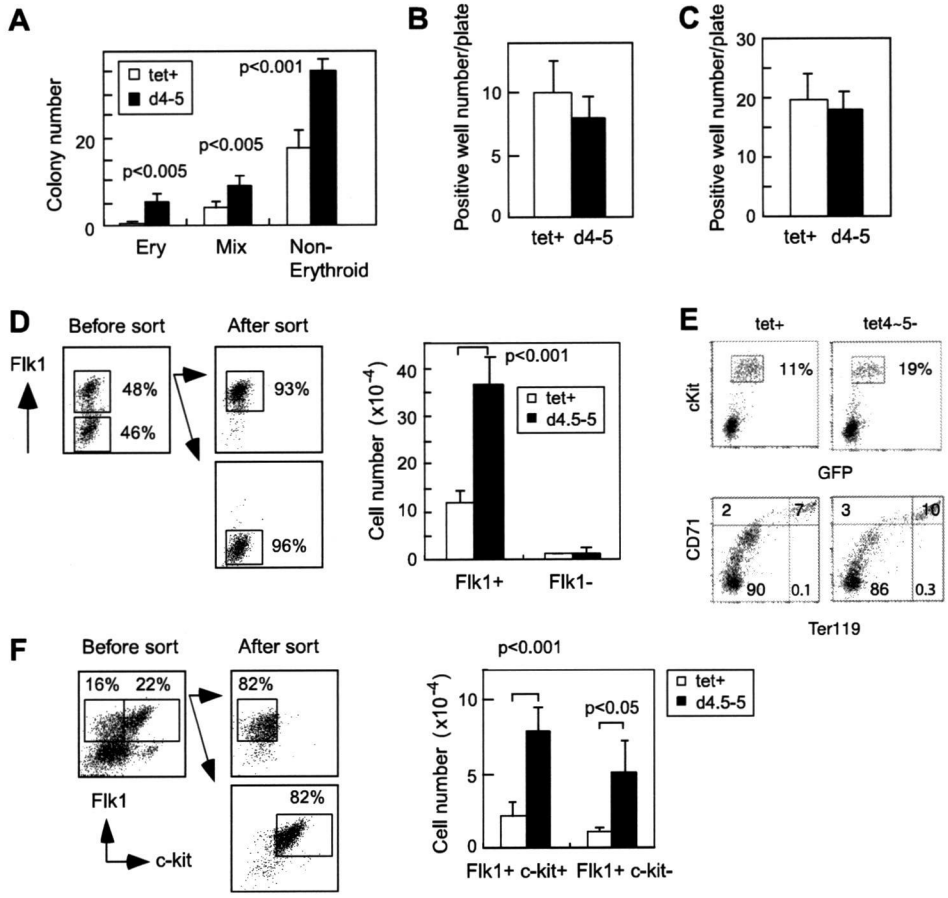

Figure 3. Unaffected hemogenic cell number by functional Runx1 expression. (**A**) The appearance of hematopoietic cells from day 6 loosely attached cells by cRunx1 expression. Cells were differentiated as in Figure 4, and both the floating and loosely attached cells were collected on day 5 and subjected to methylcellulose analysis. The colonies were evaluated based on morphology and counted after 8 days (n = 6). (**B**) The appearance of hematopoietic cells from day 5 adherent cells by cRunx1 expression. cRunx1-inducible embryonic stem (ES) cells were cultured on OP9 cells, tetracycline was removed during days 4 to 5, and the differentiated cells were dissociated by trypsinization on day 5 and replated on a 96-well plate containing OP9 stromal cells. The hematopoietic progenitor cells (HPC)–containing wells were counted on day 9. The number of HPC-positive wells from plates seeded at 5×10^2 cells/plate is shown. (**C**) The appearance of hematopoietic cells from day 4 cells induced by cRunx1 expression. The differentiated cells were dissociated by trypsinization on day 4 and replated on a 96-well plate containing OP9 stromal cells, and tetracycline was removed during days 4 to 5. The HPC-containing wells were examined as in (**B**). Results from plates seeded at 10^3 cells/plate are shown. (**D**) Effect of cRunx1 expression on $Flk1^+$ and $Flk1^-$ cells. cRunx1-inducible ES cells were differentiated on OP9 cells, and the $Flk1^+$ and $Flk1^-$ populations were isolated on day 4 by sorting. Cells were plated on a fresh OP9 layer at 2×10^4 cells/well on day 4.5 in the absence of tetracycline to induce cRunx1 expression. The induction was terminated on day 5 and the cells were counted on day 12 (n = 6). (**E**) Fluorescein-activated cell sorting (FACS) analysis of HPCs derived from $Flk1^+$ cells. The generated HPCs from $Flk1^+$ cell in (**D**) were harvested at day 12 and stained by c-kit or double-stained by CD71 and Ter119. (**F**) Effects of cRunx1 expression on $Flk1^+c\text{-}Kit^-$ and $Flk1^+c\text{-}Kit^+$. The differentiated cells were harvested on day 4 and sorted into $Flk1^+c\text{-}Kit^-$ and $Flk1^+c\text{-}Kit^+$ populations. The cells were plated at 2×10^4 cells/well on day 4.5. cRunx1 expression was induced during days 4.5 to 5 as in (**D**) and the cells were counted on day 12 (n = 6).

HPC-containing wells was observed (Fig. 3C). Together, these results demonstrate that the number of hemogenic cells is not increased by cRunx1. Given these data, we asked whether cRunx1 regulates the production of HPCs from hemogenic cells or the proliferation of HPCs, or both.

To address this question, we isolated and examined the $Flk1^+$ cell population, which is assumed to contain hemogenic cells, by sorting on day 4 (Fig. 3D). The sorted cells were then reseeded onto an OP9 cell layer and cRunx1 expression was induced for 18 hours. HPCs were detected almost exclusively in the $Flk1^+$ cell fraction without the expression of cRunx1, as reported previously [26]. When cRunx1 was expressed in the $Flk1^+$ cells, HPC production increased threefold. However, this increase was not observed in the $Flk1^-$ population, indicating that Runx1 acts specifically on $Flk1^+$ cells. The hematopoietic cells in $Flk1^+$ population were analyzed at day 12 (Fig. 3E). The frequency of the cells with the immature marker c-kit did not show significant differences between cRunx1-expressed and control cells. The CD71 and Ter119 expression which were the markers for erythroid maturation was also similar between them.

Table 1. The genes up-regulated by cRunx1 expression

Microarray ID	cRunx1/control	GeneBank ID	Gene Symbol	Description	†Hematopoietic (H) or Endothelial (E) Related Genes
94728_f_at	259.01	X68803	Mcpt1	Mast cell protease 1	H
96273_at	125.59	AI841709		EST, similarity not reported	
99958_at	86.42	J05177	Mcpt2	Mast cell protease 2	H
102733_at	56.62	M22527	Gzmc	cytotoxic T lymphocyte-specific serine protease CCPII gene	H
94729_r_at	41	X68803	Mcpt1	Mast cell protease 1	H
160623_at	33.66	AI847045		EST, similarity not reported	
102258_at	32.58	AF062476	Stra6	Stimulated by retinoic acid gene 6	
102877_at	29.87	M12302	Gzmb	Granzyme B	H
96588_at	28	D10204	Ptger3	Prostaglandin E receptor EP3 subtype	
99040_at	26.32	X66119	Slc6a4	5-hydroxytryptamine (serotonin) transporter	
161447_f_at	10.77	AV355157		EST, similarity not reported	
98420_at	10.7	AA919924		putative MYO-INOSITOL MONOPHOSPHATASE 2	
93106_i_at	8.66	M20878	Tcrb-J	T-cell receptor beta-chain mRNA, VDJ region, clone 7.9R.	H
161319_at	8.17	AV091858		EST, similarity not reported	
161020_r_at	8.06	AI508500		EST, similarity not reported	
97763_at	7.32	AB002663	Ncf1	p47phox	H
161817_f_at	6.89	AV376312		EST, similarity not reported	
102383_at	6.16	AW048977		EST, similarity not reported	
92222_f_at	5.8	U96752	H2-Q1	Histocompatibility 2, Q region locus 1	
94278_at	5.47	D37837	Lcp1	65-kDa macrophage cytosolic protein	H
92992_i_at	5.46	AI324972		EST, similarity not reported	
104032_at	5.44	AI850087		EST, similarity not reported	
161013_f_at	5.05	AI596360		EST, similarity not reported	
103539_at	4.87	X55663	Tec	Cytoplasmic tyrosine kinase, Dscr28C related (Drosophila)	H
102009_at	4.85	AI835274		EST, similarity not reported	
92406_at	4.78	D31956	Cd7	CD7 antigen	H
102272_at	4.65	AF060982	Cd160	natural killer cell BY55 precursor	H
96356_at	4.58	AW214725		EST, similar to ARP2/3 COMPLEX 41 KD SUBUNIT	
161914_s_at	4.57	AV122642		EST, similarity not reported	
104093_at	4.53	D49691	Lsp1	p50b (identical to LSP1 and pp52)	H
104541_at	4.51	U43525	Prtn3	Proteinase 3	
102708_at	4.31	U67065	Btn1a1	Butyrophilin	
96735_at	4.31	AW049732		EST, similarity not reported	
95056_r_at	4.20	AW122747		EST, similarity not reported	
93428_at	4.09	AW121806		EST, similarity not reported	
96643_at	3.97	AW121336		EST, similarity not reported	
94774_at	3.86	M31418	Ifi202b	Interferon activated gene 202	
93744_at	3.82	AI119347		EST, similar to CALM_PLAFA P24044 CALMODULIN	
102742_g_at	3.78	M18775	Mapt	Microtubule-associated protein tau	
94835_f_at	3.70	M28739	Tubb2a	Tubulin, beta 2	
92483_g_at	3.65	AF006466	Fmnl1	lymphocyte specific formin related protein (Fr1)	H
93864_s_at	3.62	U72521	Enah	Enabled homolog (Drosophila)	
93397_at	3.59	U56819	Ccr2	mcp-1 receptor	H
160995_at	3.54	AI425994		EST, similarity not reported	
99957_at	3.46	X72795	Mmp9	Matrix metalloproteinase 9	
92421_at	3.46	AI846645		EST, similarity not reported	
102641_at	3.45	L03215	Sfpi1	SFFV proviral integration 1	H
98445_at	3.42	AW125311		EST, similarity not reported	
92796_at	3.39	J02980	Alpl	Alkaline phosphatase 2	
104138_at	3.32	AW125119		EST, similarity not reported	
101501_r_at	3.26	D87973	Impact	Imprinted and ancient	
93193_at	3.24	X15643	Adrb2	Adrenergic receptor, beta 2	
100024_at	3.24	AI641895		EST, similarity not reported	
161741_r_at	3.24	AV316991		EST, similarity not reported	

(*continued*)

Table 1 (*continued*)

Microarray ID	cRunx1/control	GeneBank ID	Gene Symbol	Description	†Hematopoietic (H) or Endothelial (E) Related Genes
101561_at	3.18	K02236	Mt2	Metallothionein 2	
98952_at	3.17	AW120971		EST, similarity not reported	
92449_at	3.07	AF002701	Gfra2	Glial cell line derived neurotrophic factor family receptor alpha 2	
93573_at	3.06	J00605	Mt1	Metallothionein 1	
101850_at	3.06	Z46299	Spa17	Sp17 gene for sperm specific protein	
101851_at	3.03	AF029215	Cd200	Antigen identified by monoclonal antibody MRC OX-2	

†Genes related either to hematopoietic or to endothelial cells were selected from the lists. The selected genes were preferentially expressed in and have important functions for each cell type.

We further pinpointed the timing of cRunx1 function by isolating the Flk1$^+$c-Kit$^+$ and Flk1$^+$c-Kit$^-$ fractions on day 4. As shown in Figure 3E, cRunx1 expression increased the number of HPCs produced from Flk1$^+$c-Kit$^+$ and Flk1$^+$c-Kit$^-$ cells to similar extents. Flk1$^+$c-Kit$^+$ cells are assumed to be in the earliest stage of hematopoietic commitment [27]; therefore, the double-positive and Flk1$^+$c-Kit$^-$ cell fractions contain recently emerged HPCs and cells just becoming HPCs, respectively. Taking this information into account, peak cRunx1 function occurs just around the emergence of the hematopoietic progenitors. Thus, the target cells of cRunx1 are HPCs or their hemogenic precursors, or both. In the case of hemogenic precursors being the target cells, cRunx1 increases the efficiency of HPC emergence from hemogenic cells.

Gene expression profile in the course of cRunx1 expression

To elucidate the target molecules of Runx1 expression, which are presumably involved in the production of definitive progenitor cells, we performed DNA microarray analysis. Flk1$^+$ckit$^+$ cells were prepared on day 4, cRunx1 was induced for 18 hours, and RNA was isolated to compare the expression profiles of the experimental and control cells. Tables 1 and 2 showed lists of the genes that were upregulated and downregulated more than threefold, respectively. The genes preferentially expressed in or have important roles in hematopoietic cells and endothelial cells were marked as H or E, respectively, in the right column of the tables. There are no endothelial cell related genes in 36 upregulated genes (Table 1), but 13 genes in 50 downregulated genes (described "E" at the right column in Table 2), which is significantly different ($p < 0.005$ by χ^2 test). EST sequences that did not appear on National Center for Biotechnology Information EST database with any similarity with known genes were excluded from comparison. The genes appeared more than once were counted once. To the contrary, there are 14 and 10 hematopoietic cell–related genes among up- and downregulated genes, respectively (described "H" in Table 1 and 2). The expression of several endothelial cell-specific genes, *Emcn, Icam2, Edn1, Kdr (Flk-1)*, a reported Runx1 target gene [28], was confirmed by reverse transcription PCR (Fig. 4). T-cell–related genes (*Gzmc, Gzmb, Tcrb-J, Tec, Cd7, Cd160*) and erythrocyte-related genes (*Hbb-b2, Hbb-bh3, Hbb-y, Hba-a1, Rhag*) were categorized in the upregulated and downregulated groups, respectively. Two genes important for both early hematopoiesis and blood cell maturation, CBF (runx1 itself) and sfpi1 (pu.1), were identified as down- and upregulated genes, respectively.

Discussion

We demonstrated that the number of hematopoietic progenitors was increased by cRunx1 expression. Considering that the number of hemogenic cells was not increased by cRunx1, Runx1 serves to promote either the proliferation of immature HPCs or the emergence of HPCs from hemogenic cells, or both. In fact, we have shown that Flk1$^+$c-Kit$^+$ and Flk1$^+$c-Kit$^-$ cells are the targets of cRunx1 expression. The previous reports describing that the G1-entry promoting function of AML1 (i.e., human Runx1) and promoting cell proliferation by cyclin-dependent phosphorylation of Runx1 were supportive for the notion that proliferation of immature progenitors was stimulated by Runx1 [29,30]. Meanwhile, accumulation of immature HPCs was previously observed in adult conditional *Runx1* knockout mice, suggesting that Runx1 plays a role in promoting hematopoietic differentiation [31,32]. However, block of proliferation of immature cells was not detected in adult knockout mice. Taken together with our data, we prefer the notion that runx1 promotes the emerging of hematopoietic cells from endothelial cells during embryonic hematopoietic stage.

In our experiment, the induction of Runx1 expression in Flk1$^-$ cells, which are nonhemogenic, did not affect HPC production (Fig. 3D). In addition, our clonal analysis at the single hemogenic cell level revealed that the increased number of hemogenic cells was not caused by Runx1 induction (Fig. 3B, C). Thus, it is unlikely that the

Table 2. The genes down-regulated by cRunx1 expression.

MicroarrayID	cRunx1/control	GeneBankID	GeneSymbol	Description	†Hematopoietic (H) or Endothelial (E) Related Genes
92289_at	0.017	X58289	Ptprb	Protein tyrosine phosphatase, receptor type, B	E
92997_g_at	0.021	D49473	Sox17	SRY-box containing gene 17	
95546_g_at	0.041	X04480	Igf1	Insulin-like growth factor 1	
93885_g_at	0.042	AB034693	Emcn	endomucin-1	E
104729_at	0.044	X57971	Gja4	Gap junction membrane channel protein alpha 4	E
94997_at	0.071	AF060883	Emcn	endomucin	E
104516_at	0.076	U82758	Cldn5	lung-specific membrane protein	E
93454_at	0.082	AF081789	Cd93	cell surface antigen AA4 (AA4)	H
99053_at	0.085	X65493	Icam2	Intercellular adhesion molecule 2	E
99914_at	0.093	U43715	Hand2	Heart and neural crest derivatives expressed transcript 2	
99893_at	0.103	AF020737	Fgf13	Fibroblast growth factor 13	
92372_at	0.103	X80992	Bmp6	Bone morphogenetic protein 6	
96912_s_at	0.104	X15591	Ctla2a	Cytotoxic T lymphocyte-associated protein 2 alpha	H
92899_at	0.109	D42051	Gad2	Glutamate Decarboxylase	
97771_r_at	0.114	AA733372		EST, similarity not reported	
94712_at	0.114	U73620	Vegfc	Vascular endothelial growth factor C	
103226_at	0.117	Z11974	Mrc1	Mannose receptor, C type 1	
103518_at	0.118	X15592	Ctla2b	Cytotoxic T lymphocyte-associated protein 2 beta	H
92996_at	0.128	D49473	Sox17	SRY-box containing gene 17	
104146_at	0.131	AI853551		EST, similarity not reported	
103534_at	0.141	V00722	Hbb-b2	beta-1-globin	H
99444_at	0.145	AJ250490	Ramp2	receptor activity modifying protein 2 (Ramp2 gene)	
96132_at	0.157	AB023957	Apcdd1	EIG 180 mRNA for ethanol induced gene product	
103532_at	0.166	AW120579		EST, similarity not reported	
102639_at	0.168	AB011451	Chst2	N-acetylglucosamine-6-O-sulfotransferase	E
101991_at	0.168	D16215	Fmo1	flavin-containing monooxygenase	
98320_at	0.171	Y12657	Cyp26a1	Cytochrome P450, 26, retinoic acid	
102737_at	0.176	U35233	Edn1	Endothelin 1	E
104239_at	0.178	AW208513		EST, similarity not reported	
101063_at	0.179	M29793	Tnnc1	slow/cardiac troponin C (cTnC)	
103412_at	0.186	AI847230		EST, similarity not reported	
100414_s_at	0.188	X15313	Mpo	Myeloperoxidase	H
161001_at	0.189	AV367683		EST, similarity not reported	
92652_at	0.191	AF030001		major histocompatibility locus class III region-butyrophilin-like protein gene, partial cds; Notch4, PBX2, RAGE, lysophatidic acid acyl transferase-alpha, palmitoyl-protein thioesterase 2 (PPT2), CREB-RP, and tenascin X	
93880_at	0.191	AB031037	Eomes	Tbr2	
95671_at	0.199	AJ243895	Hey1	basic-helix-loop-helix protein (Hey1 gene)	
103743_at	0.200	AI851348		EST, similarity not reported	
103499_at	0.202	AI843063		EST, similarity not reported	
92506_at	0.204	AF098460	Hapln1	link protein	
98423_at	0.209	M81445	Gjb2	Gap junction membrane channel protein beta 2	
97235_f_at	0.210	AW124988		EST, similarity not reported	
104201_at	0.214	AA718649		EST, similarity not reported	
97795_at	0.215	AB015595	Calcrl	calcitonin receptor-like receptor precursor	E
102720_at	0.220	X71426	Tek	Endothelial-specific receptor tyrosine kinase	E
161099_at	0.227	AA285978		EST, similarity not reported	
161236_r_at	0.228	AV266956		EST, similarity not reported	
103535_at	0.232	X14061	Hbb-bh3	Hemoglobin beta, pseudogene bh3	H
94935_at	0.238	AI843739		EST, similarity not reported	
100724_at	0.241	M36516	Zfp28	Zinc finger protein 28	
100134_at	0.243	X77952	Eng	Endoglin	E
92399_at	0.244	D26532	Runx1	Core binding factor alpha 2	
92487_at	0.244	AB023419	Sox7	mSox7	E
97180_f_at	0.248	V00726	Hbb-y	germ line gene coding for beta-globin (Y2)	H
104265_at	0.261	X70842	Kdr	Kinase insert domain protein receptor	E
104697_at	0.269	AW121127		EST, similarity not reported	

(continued)

Table 2 (*continued*)

MicroarrayID	cRunx1/control	GeneBankID	GeneSymbol	Description	†Hematopoietic (H) or Endothelial (E) Related Genes
94781_at	0.272	V00714	Hba-a1	Hemoglobin alpha, adult chain 1	H
103977_at	0.272	AF087644	F10	Coagulation factor X	
95083_at	0.281	X81581	Igfbp3	Insulin-like growth factor binding protein 3	
100778_at	0.284	L11332	Cd38	CD38 antigen	H
93912_at	0.289	AW047616		EST, similarity not reported	
92273_at	0.289	U49853	Ptpn18	Protein tyrosine phosphatase, non-receptor type 18	
102762_r_at	0.289	AF057527	Rhag	erythrocyte membrane protein Rh50 (Rhag) gene	H
92945_at	0.291	L32372	Gria2	Glutamate receptor, onotropic, AMPA2 (alpha 2)	
94189_at	0.294	AB011665	Bcl6b	BAZF	
92192_s_at	0.296	D12619	Pcsk5	Proprotein convertase subtilisin/kexin type 5	
161184_f_at	0.298	AV235418		EST, similar to TIE receptor tyrosine kinase	E
102957_at	0.299	U20159	Lcp2	76 kDa tyrosine hosphoprotein SLP-76	

†Genes related either to hematopoietic or to endothelial cells were selected from the lists. The selected genes were preferentially expressed in and have important functions for each cell type.

production of hemogenic cells from nonhemogenic cells is induced by Runx1 at this time point. Considering the complete loss of definitive hematopoiesis in *Runx1*-null mice, it is likely that *Runx1* functions earlier, during the determination of cell fate. Recently, it was shown that cells with hematopoietic stem cells potential could be originated in *Runx1*-expressing yolk sac cells, which migrate to organs where subsequent definitive hematopoiesis occurs, indicating that hematopoietic cell fate is specified long before emergence of definitive hematopoiesis [33]. Our finding that *Runx1* expression in nonhemogenic cells did not provide hemogenic potency during days 4 and 5 indicates that Runx1 is not involved in the induction of hemogenic cells. Instead, the major contribution of runx1 in this period would be enhancement of the appearance of hematopoietic cells from endothelial cells. It is surmisable that a large-scale alteration of gene expression must occur to expose the drastic phenotypic change, such as loss of cell-to-cell junction during transition to hematopoietic cells. Runx1 might be involved in the gene-regulation process as we discuss later. In previous studies, strong Runx1 expression was detected in intraaortic hematopoietic clusters attached to luminal endothelial cells, as well as in the underlying endothelial and mesenchymal cells [34]. We propose that part of the function of Runx1 in these intraaortic hematopoietic clusters is to support or promote the increase of immature progenitors, either in a cell-autonomous manner, such as in suppression of endothelial characteristics, or in a nonautonomous manner, such as in secretion of some cytokines.

We found that expression of several endothelial-specific genes was downregulated by induction of c*Runx1* for even a relatively short period (18 hours). One possibility is that the number of endothelial cells was decreased by the preferential differentiation of hematopoietic cells following induction of cRunx1, and subsequently the amount of endothelial-specific mRNA was reduced. However, this is unlikely because induction of the hemogenic fate was not caused by c*Runx1* expression (Fig. 3). We prefer a different interpretation, namely that hematopoietic cells rapidly lose their ability to acquire endothelial characteristics during the course of their development from progenitors, and that

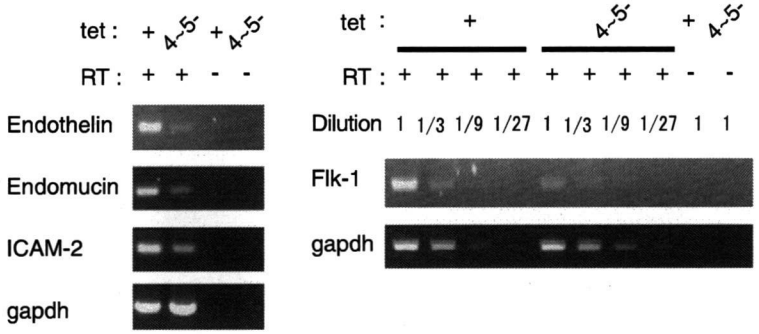

Figure 4. Suppression of endothelial-specific genes by Runx1. Reverse transcription analysis of genes downregulated by Runx1. cRunx1 expression was induced for 18 hours in the Flk1$^+$c-Kit$^+$ population purified on day 4 of differentiation. RNA was isolated from the induced cells and noninduced control cells and subjected to reverse transcription polymerase chain reaction.

Runx1 plays a major role in suppression of endothelial-specific genes during this process.

Pu.1, one of the direct target genes of runx1 and critical for hematopoiesis, was listed among upregulated genes by our experimental system [35]. It is likely that the runx1-pu.1 pathway would be the cause of increase of immature progenitors. It was unexpected that runx1 was one of the downregulated genes, because positive feedback mechanism was, conversely, suggested from the study in lacZ-knockin mice [36]. Considering that runx1 plays critical roles in hematopoietic development, its expression level should be regulated in a highly controlled manner. In fact, runx1 level is controlled both transcriptionally and posttranscriptionally, and runx1 by itself regulates microRNA expression [37]. Taken together, it is possible that the high induced mRNA level of runx-1 would be compensated by downregulation of the endogenous mRNA by some unknown mechanisms. It was also notable that Sox17 was found as a downregulated gene, because Sox17 is recently reported to be important for fetal hematopoietic stem cells function [38]. However, Sox17 is a well-known determinant of endoderm cell fate (reviewed in [39]). Our observation that endothelial-related genes were suppressed implies that runx1 would have a function to suppress the genes necessary for lineages other than hematopoietic cells.

Acknowledgments

We thank Dr. T. Kina (Kyoto University), Dr. S. Akira (Osaka University), Morinaga Milk Co., and Kirin Brewery Co. for providing instruments and materials. We also thank Ms. T. Asada and A. Mizokami for their assistance. This study was supported in part by grants from the Ministry of Education, Science, Sports, and Culture and the 21st Century Center of Excellence (CICET). E.S. and T.N. designed the research, E.S. and A.S. performed research, E.S., K.K. and T.N wrote the article.

References

1. Choi K, Kennedy M, Kazarov A, Papadimitriou JC, Keller G. A common precursor for hematopoietic and endothelial cells. Development. 1998;125:725–732.
2. Jaffredo T, Gautier R, Eichmann A, Dieterlen-Lievre F. Intraaortic hemopoietic cells are derived from endothelial cells during ontogeny. Development. 1998;125:4575–4583.
3. Sugiyama D, Ogawa M, Hirose I, Jaffredo T, Arai K, Tsuji K. Erythropoiesis from acetyl LDL incorporating endothelial cells at the preliver stage. Blood. 2003;101:4733–4738.
4. Nishikawa S-I, Nishikawa S, Kawamoto H, et al. In vitro generation of lymphohematopoietic cells from endothelial cells purified from murine embryos. Immunity. 1998;8:761–769.
5. Fehling HJ, Lacaud G, Kubo A, et al. Tracking mesoderm induction and its specification to the hemangioblast during embryonic stem cell differentiation. Development. 2003;130:4217–4227.
6. Lacaud G, Robertson S, Palis J, Kennedy M, Keller G. Regulation of hemangioblast development. Ann N Y Acad Sci. 2001;938:96–107. discussion 108.
7. Ogawa M, Fraser S, Fujimoto T, Endoh M, Nishikawa S, Nishikawa SI. Origin of hematopoietic progenitors during embryogenesis. Int Rev Immunol. 2001;20:21–44.
8. Kennedy M, Firpo M, Choi K, et al. A common precursor for primitive erythropoiesis and definitive hematopoiesis. Nature. 1997;386:488–493.
9. Endoh M, Ogawa M, Orkin S, Nishikawa S. SCL/tal-1-dependent process determines a competence to select the definitive hematopoietic lineage prior to endothelial differentiation. EMBO J. 2002;21: 6700–6708.
10. Bae SC, Yamaguchi-Iwai Y, Ogawa E, et al. Isolation of PEBP2 alpha B cDNA representing the mouse homolog of human acute myeloid leukemia gene, AML1. Oncogene. 1995;8:809–814.
11. de Bruijn MF, Speck NA. Core-binding factors in hematopoiesis and immune function. Oncogene. 2004;23:4238–4248.
12. Ogawa E, Inuzuka E, Maruyama M, et al. Molecular cloning and characterization of PEBP2 beta, the heterodimeric partner of a novel Drosophila runt-related DNA binding protein PEBP2 alpha. Virology. 1993;194:314–331.
13. Wang S, Wang Q, Crute BE, Melnikova IN, Keller SR, Speck NA. Cloning and characterization of subunits of the T-cell receptor and murine leukemia virus enhancer core-binding factor. Mol Cell Biol. 1993;13:3324–3339.
14. Kitabayashi I, Yokoyama A, Shimizu K, Ohki M. Interaction and functional cooperation of the leukemia-associated factors AML1 and p300 in myeloid cell differentiation. EMBO J. 1998;17:2994–3004.
15. Levanon D, Goldstein RE, Bernstein Y, et al. Transcriptional repression by AML1 and LEF-1 is mediated by the TLE/Groucho corepressors. Proc Natl Acad Sci U S A. 1998;95:11590–11595.
16. Lutterbach B, Westendorf JJ, Linggi B, Isaac S, Seto E, Hiebert SW. A mechanisms of repression by acute myeloid leukemia-1, the target of multiple chromosomal translocations in acute leukemia. J. Biol. Chem. 2000;275:651–656.
17. Wang Q, Stacy T, Binder M, Marin-Padilla M, Sharpe AH, Speck NA. Disruption of the Cbfa2 gene causes necrosis and hemorrhaging in the central nervous system and blocks definitive hematopoiesis. Proc Natl Acad Sci U S A. 1996;93:3444–3449.
18. Okuda T, van Deursen J, Hiebert SW, Grosveld G, Downing JR. AML1, the target of multiple chromosomal translocations in human leukemia, is essential for normal fetal liver hematopoiesis. Cell. 1996;84:321–330.
19. Era T, Witte ON. Regulated expression of P210 Bcr-Abl during embryonic stem cell differentiation stimulates multipotential progenitor expansion and myeloid cell fate. Proc Natl Acad Sci U S A. 2000;97:1737–1742.
20. Kitajima K, Masuhara M, Era T, Enver T, Nakano T. GATA-2 and GATA-2/ER display opposing activities in the development and differentiation of blood progenitors. EMBO J. 2002;21:3060–3069.
21. Nakano T, Kodama H, Honjo T. Generation of lymphohematopoietic cells from embryonic stem cells in culture. Science. 1994;265: 1098–1101.
22. Nakano T, Kodama H, Honjo T. In vitro development of primitive and definitive erythrocytes from different precursors. Science. 1996;272: 722–724.
23. Kanno T, Kanno Y, Chen LF, Ogawa E, Kim WY, Ito Y. Intrinsic transcriptional activation-inhibition domains of the polyomavirus enhancer binding protein 2/core binding factor alpha subunit revealed in the presence of the beta subunit. Mol Cell Biol. 1998;18:2444–2454.
24. Kagoshima H, Akamatsu Y, Ito Y, Shigesada K. Functional dissection of the alpha and beta subunits of transcription factor PEBP2 and the redox susceptibility of its DNA binding activity. J Biol Chem. 1996; 271:33074–33082.
25. Fujita Y, Nishimura M, Taniwaki M, Abe T, Okuda T. Identification of an alternatively spliced form of the mouse AML1/RUNX! gene transcript AML1c and its expression in early hematopoietic development. Biochem Biophys Res Commun. 2001;281:1248–1255.
26. Faloon P, Arentson E, Kazarov A, et al. Basic fibroblast growth factor positively regulates hematopoietic development. Development. 2000; 127:1931–1941.

27. Willey S, Ayuso-Sacido A, Zhang H, et al. Acceleration of mesoderm development and expansion of hematopoietic progenitors in differentiating ES cells by the mouse Mix-like homeodomain transcription factor. Blood. 2006;107:3122–3130.
28. Hirai H, Samokhvalov IM, Fujimoto T, Nishikawa S, Imanishi J, Nishikawa S. Involvement of Runx1 in the down-regulation of fetal liver kinase-1 expression during transition of endothelial cells to hematopoietic cells. Blood. 2005;106:1948–1955.
29. Bernardin F, Friedman AD. AML1 stimulates G1 to S progression via its transactivation domain. Oncogene. 2002;21:3247–3252.
30. Strom DK, Nip J, Westendorf JJ, et al. Expression of the AML-1 oncogene shortens the G(1) phase of the cell cycle. J Biol Chem. 2000;275: 3438–3445.
31. Ichikawa M, Asai T, Saito T, et al. AML-1 is required for megakaryocytic maturation and lymphocytic differentiation, but not for maintenance of hematopoietic stem cells in adult hematopoiesis. Nat Med. 2004;10:299–304.
32. Growney JD, Shigematsu H, Li Z, et al. Loss of Runx1 perturbs adult hematopoiesis and is associated with a myeloproliferative phenotype. Blood. 2005;106:494–504.
33. Samokhvalov IM, Samokhvalov NI. Nishikawa S-I. Cell tracing shows the contribution of the yolk sac to adult hematopoiesis. Nature. 2007; 446:996–997.
34. North TE, de Bruijn MF, Stacy T, et al. Runx1 expression marks long-term repopulating hematopoietic stem cells in the midgestation mouse embryo. Immunity. 2002;16:661–672.
35. Huang G, Zhang P, Hirai H, et al. PU.1 isw a major downstream tsrget of AML1(RUNX1) in adult mouse hematopoiesis. Nat Genet. 2008; 40:51–60.
36. North T, Gu TL, Stacy T, et al. Cbfa2 is required for the formation of intra-aortic hematopoietic clusters. Development. 1999;126:2563–2575.
37. Fontana L, Pelosi E, Greco P, et al. MicroRNAs 17-5p-20a-106a control monocytopoiesis through AML1 targeting and M-CSF receptor upregulation. Nat Cell Biol. 2007;9:775–787.
38. Kim I, Saunders TL, Morrison SJ. Sox17 dependence distinguishes the transcriptional regulation of fetal from adult hematopoietic stem cells. Cell. 2007;130:470–483.
39. Tam PP, Kanai-Azuma M, Kanai Y. Early endoderm development in vertebrates: lineage differentiation and morphogenetic function. Curr Opin Genet Dev. 2003;13:393–400.

NOTE · *Anatomy*

Site-Dependent Differences in Collagen Lamellae in the Corneal Substantia Propria of Beagle Dogs

Aya NAGAYASU[1)], Tomoe HIRAYANAGI[1)], Yuji TANAKA[2)], Prasarn TANGKAWATTANA[3)], Hiromi UEDA[1)] and Kazushige TAKEHANA[1)]

[1)]*Department of Veterinary Anatomy, School of Veterinary Medicine, Rakuno Gakuen University, Ebetsu, Hokkaido 069–8501,*
[2)]*Department of Ophthalmology and Visual Science Tohoku University Graduate School of Medicine, Sendai Miyagi 980–8574, Japan and*
[3)]*Department of Veterinary Anatomy, Faculty of Veterinary Medicine, Khon Kean University, Khon Kean 40002, Thailand*

(Received 27 March 2009/Accepted 30 April 2009)

ABSTRACT. The fine structure in the center and periphery of the cornea of 16 beagle dogs were characterized and compared. The central cornea (about 540 μm) was apparently thinner than the peripheral cornea (about 720 μm). Thickness ratios of the corneal substantia propria to the entire cornea were approximately 86% in both portions. In addition, number of collagen lamellae, collagen fibril diameter, and collagen fibril index of the central substantia propria are different from those of the periphery (253 vs 236 lamellae, 29.1 vs 32.0 nm, and 39.0 vs 41.6%, respectively). These differences are thought to be due to site-dependent accumulation of proteoglycans (decorin and lumican) which are responsible for production of thin fibrils. The central portion with higher proteoglycans would have abundant thin fibrils with less slippage but better elasticity to buffer against the direct impact of intraocular pressure on the cornea. In contrast, thick fibrils in the peripheral substantia propria would contribute to the maintenance of tensile strength acting on the transition zone between the cornea and sclera.

KEY WORDS: canine, collagen fibrils, collagen lamellae, cornea, corneal substantia propria.

J. Vet. Med. Sci. 71(9): 1229–1231, 2009

The general structure of the cornea has been described in many textbooks [1, 6, 17, 18]. With the recent development of technology in regenerative medicine, biomedical studies on the cornea of dogs and other animals have been increasing [11, 19, 21]. An understanding of the fine structure of the normal canine cornea is essential for the development of corneal tissue engineering for treatment of corneal diseases. The fine structure of the corneal substantia propria, which occupies approximately 90% of the entire thickness of the cornea, has not yet been completely determined. The objective of this study was to characterize and compare the fine structures in the central portion and peripheral portion of the normal corneal substantia propria of beagle dogs.

The use of experimental animals was approved by the Ethics Committee of Rakuno Gakuen University, Japan, and compliance with the NIH Guide for the Care and Use of Laboratory Animals [DHEW Publication No. (NIH) 85–23, Revised 1985, Office of Science and Health Reports, DRR/NIH, Bethesda, MD 20892]. Sixteen male beagles at the age of 16.8 ± 7.0 months with body weight of 10.7 ± 1.1 kg were used. After anesthesia with 25 mg/kg of pentobartital sodium, IV (Kyoritsu Seiyaku Corporation, Tokyo, Japan), these animals were euthanized by exsanguination. Then, the left eyeball was surgically removed from each dog. Twelve eyeballs were perfused with 10% formalin, and bisected in the median plane by using a razor blade for measurements of central and peripheral corneal thicknesses at ten sites for each sample. Four eyeballs were fixed in 3.0% glutaraldehyde in 0.1 M phosphate buffer (pH 7.4) for 24 hr at room temperature. Then, 2-mm^2 corneal samples were excised from the center and periphery of the eyeballs and post-fixed in 1.0% osmium tetroxide in 0.1 M phosphate buffer for 1 hr at room temperature. Thereafter, the samples were washed with 0.1 M phosphate buffer (pH 7.4), dehydrated in a graded ethanol series, and embedded in Quetol 812 (Nissin EM, Tokyo, Japan). Semithin sections were stained with 2.0% toluidine blue and examined by a light microscope. Thickness of the whole cornea and corneal substantia propria was measured at ten sites for each sample using Image J software (version 1.30). Thickness ratio of the substantia propria to the whole cornea was calculated. Ultrathin sections were stained with 1.0% uranyl acetate and 1.0% lead citrate and examined by a transmission electron microscope (JEM-1220; JEOL, Tokyo, Japan). In the corneal substantia propria, the averages of number and thickness of collagen lamellae were calculated and measurement of collagen fibril parameters was performed for 450 fibrils randomly selected from each sample using Image J software (version 1.30). The averages of collagen fibril diameter and collagen filbril index CFI were calculated. CFI is the percentage of area covered by collagen and represents a collagen-to-non collagen ratio in the extracellular matrix [5]. Student's *t*-test was used for data analysis and comparison between the central and peripheral portions of the cornea. Statistical significance was considered at the level of p=0.05.

Thickness of the central cornea (540.8 ± 205.5 μm) was significantly lower than that of the peripheral cornea (724.6 ± 178.3 μm) (Fig. 1). However, thickness ratio of the corneal substantia propria to the whole corneal was approximately 86% in both portions. There was no significant

* CORRESPONDENCE TO: TAKEHANA, K., Department of Veterinary Anatomy, Rakuno Gakuen University, Ebetsu, Hokkaido 069–8501, Japan.
e-mail: takechan@ rakuno.ac.jp